

Fyzikální vlastnosti materiálů

FX001

1. Vazba v pevné látce, elastické a tepelné vlastnosti materiálů
2. Elektrické vlastnosti materiálů
3. Optické vlastnosti materiálů
4. Magnetické vlastnosti materiálů
5. Supravodiče a grafen

Fyzikální vlastnosti materiálů

4. Magnetické vlastnosti materiálů

- a) Magnetismus izolovaných atomů – klasický a kvantový model diamagnetismu, paramagnetismus: klasický a kvantově mechanický model, Pauliho paramagnetismus, Van Vleckův paramagnetismus.
- b) Feromagnetika a antiferomagnetika – výměnná interakce, Heisenbergův hamiltonián, Weissova teorie středního pole, feromagnetismus prvků, slitin, sloučenin, antiferomagnetismus, ferity
- c) Elektrický transport v magnetickém poli – Hallův jev, magnetoresistance

Demagnetizační pole

	podél význačné osy	kolmo na významnou osu
koule	1/3	1/3
dlouhá tyč	0	1/2
tenká deska	1	0
rotační elipsoid	Nc	(1-Nc)/2

$$H_i = H_o - NM$$

$$B_i = \mu_0 (H_i + M) = B_o + \mu_0 (1 - N)M$$

$$N_x + N_y + N_z = 1$$

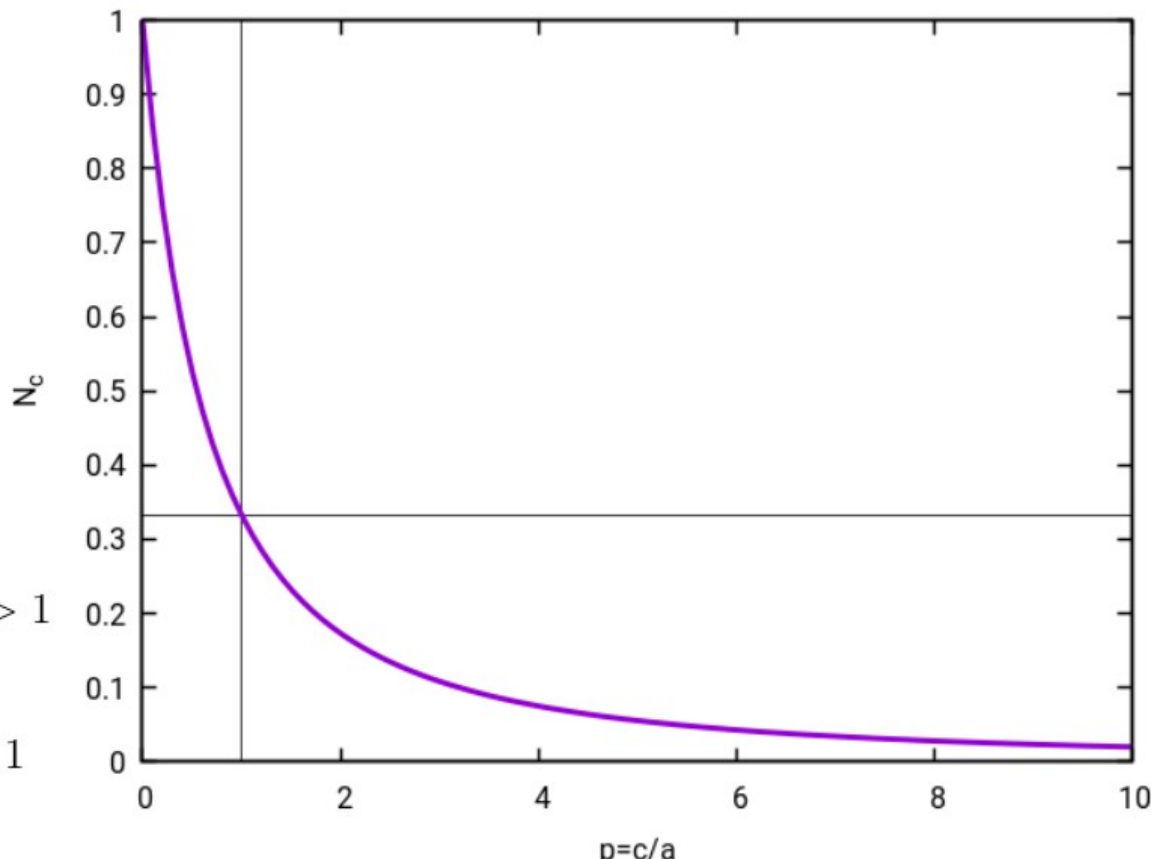
Rotační elipsoid

Demagnetizační faktor podél rotační osy c ,
délka kolmé osy a

$$p = c/a$$

$$N_c = \frac{1}{p^2 - 1} \left[\frac{p}{\sqrt{p^2 - 1}} \ln \left(p + \sqrt{p^2 - 1} \right) - 1 \right], \quad p > 1$$

$$N_c = \frac{1}{1 - p^2} \left[1 - \frac{p}{\sqrt{1 - p^2}} \arcsin \sqrt{1 - p^2} \right], \quad p < 1$$



diamagnetické materiály – susceptibilita

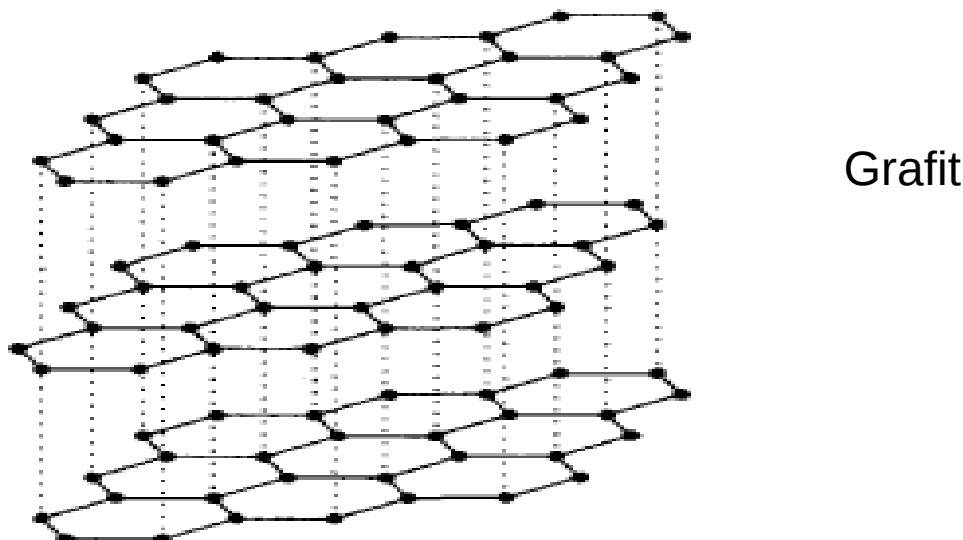
$$\chi = -\mu_0 e^2 N Z r^2 / 6m,$$

$$\chi/\rho$$

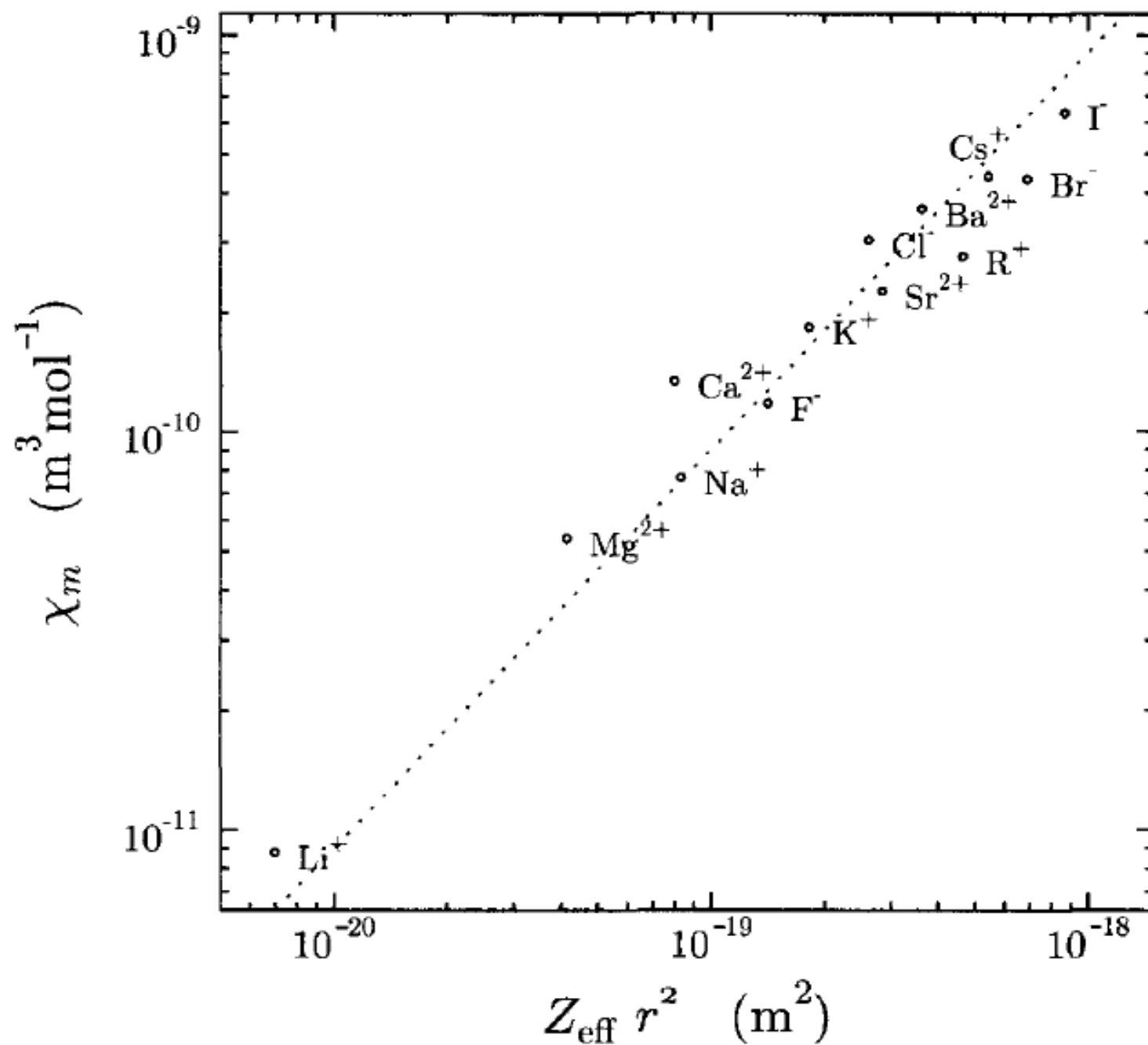
	$\chi (10^{-9})$	$\chi_{\text{mol}} (10^{-9} \text{ m}^3 \text{mol}^{-1})$	$\chi/\rho (10^{-9} \text{ m}^3 \text{kg}^{-1})$
Ne	-3.78	-0.084	-4.20
Ar	-10.8	-0.241	-6.03
Kr	-16.1	-0.361	-4.30
Xe	-24.4	-0.545	-4.15
H ₂ O	-9050	-0.163	-9.05
GaAs	-16272	-0.443	-3.06
Si	-3215	-0.0386	-1.38
Ge	-7085	-0.0966	-1.33
Cu	-9676	-0.0686	-1.08

diamagnetické materiály – susceptibilita

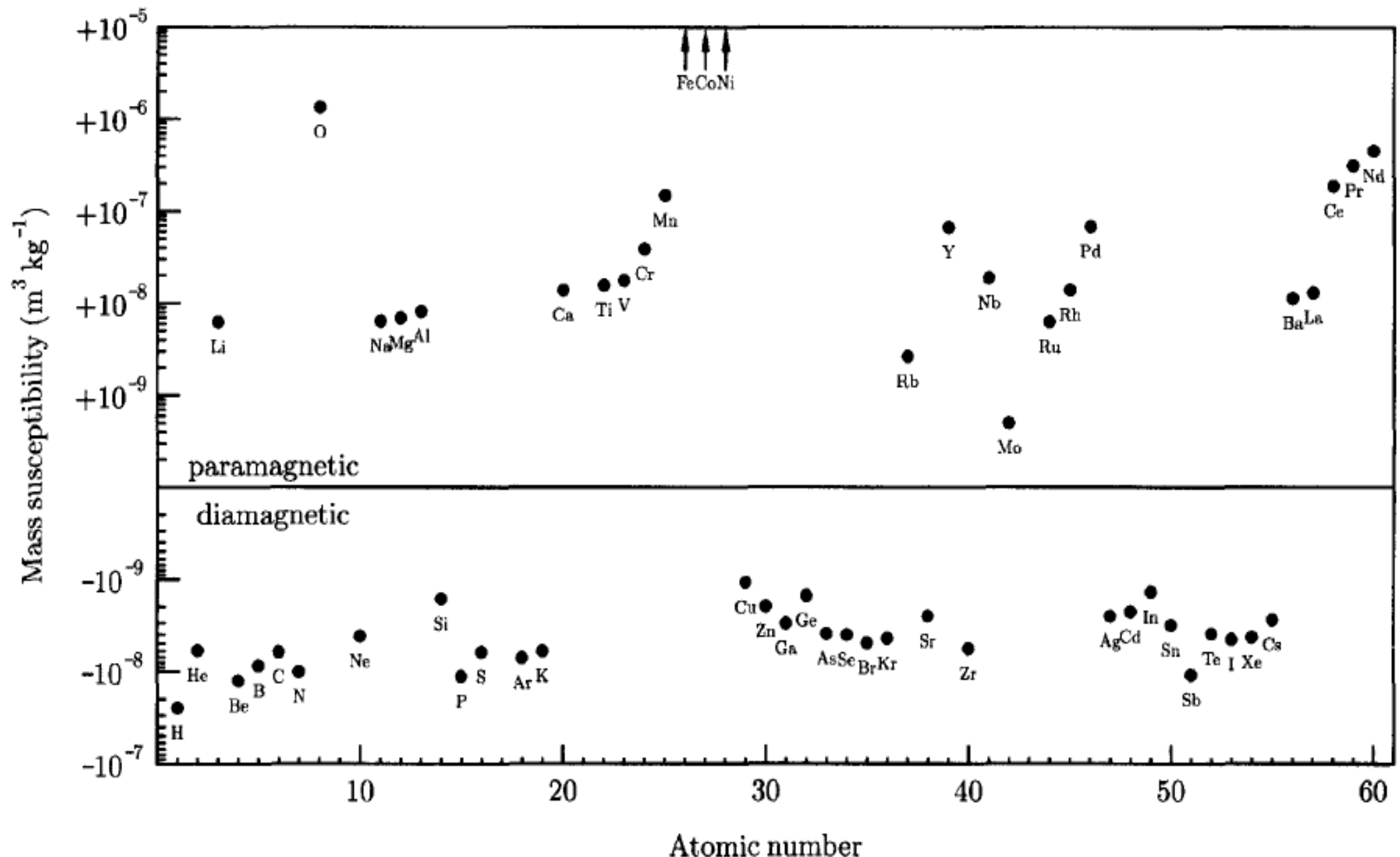
	$\chi (10^{-6})$	$\chi_{\text{mol}} (10^{-9} \text{ m}^3 \text{mol}^{-1})$	$\chi/\rho (10^{-9} \text{ m}^3 \text{kg}^{-1})$
NaF		-0.241	-5.84
NaCl		-0.366	-6.27
NaBr		-0.603	-5.9
Grafit $\chi \parallel c$	-610	-3.2	-264
Grafit $\chi \perp c$	-14	-0.075	-6.3
Bismut	-166	-3.5	-17



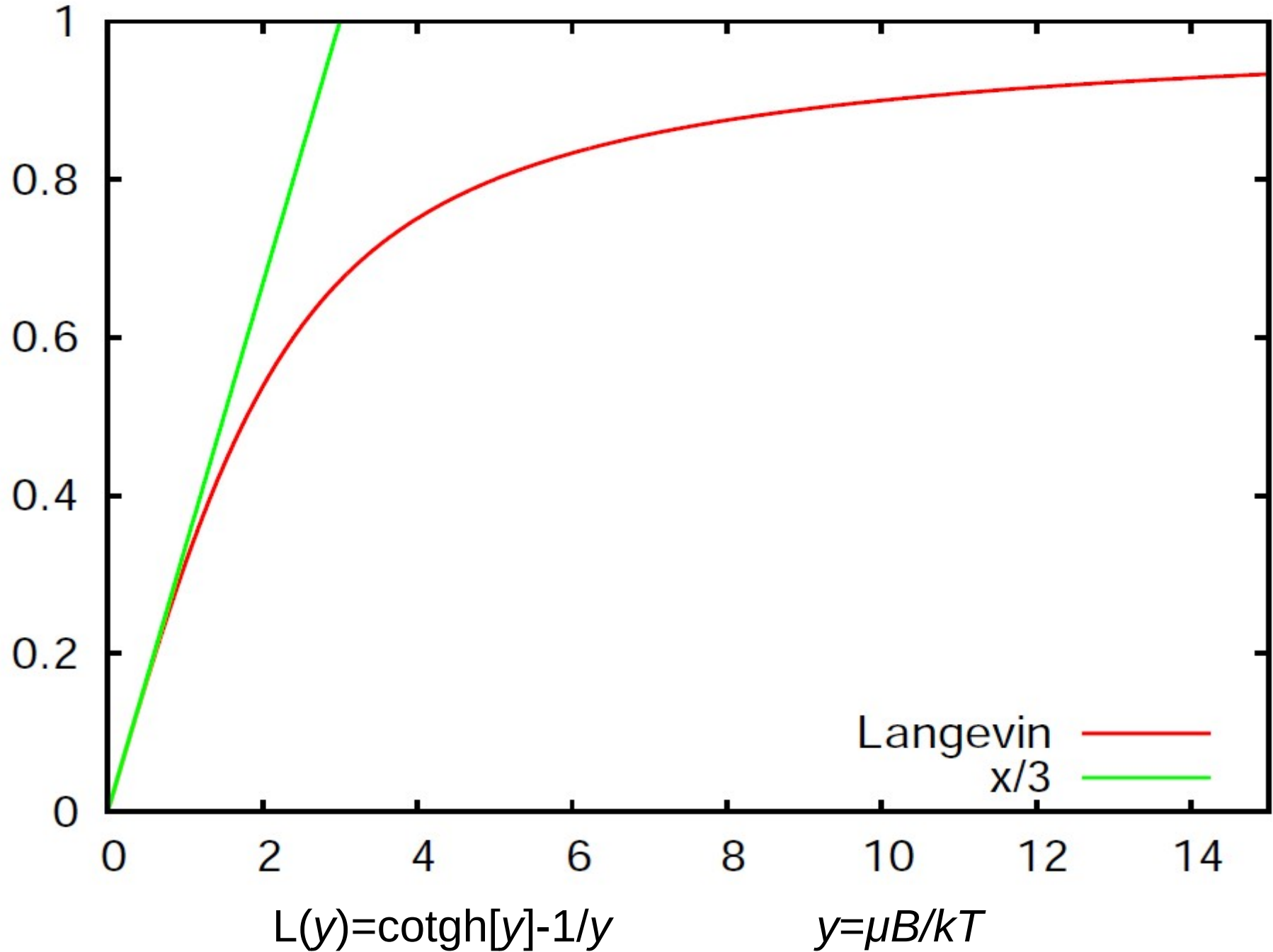
Diamagnetická susceptibilita některých iontů



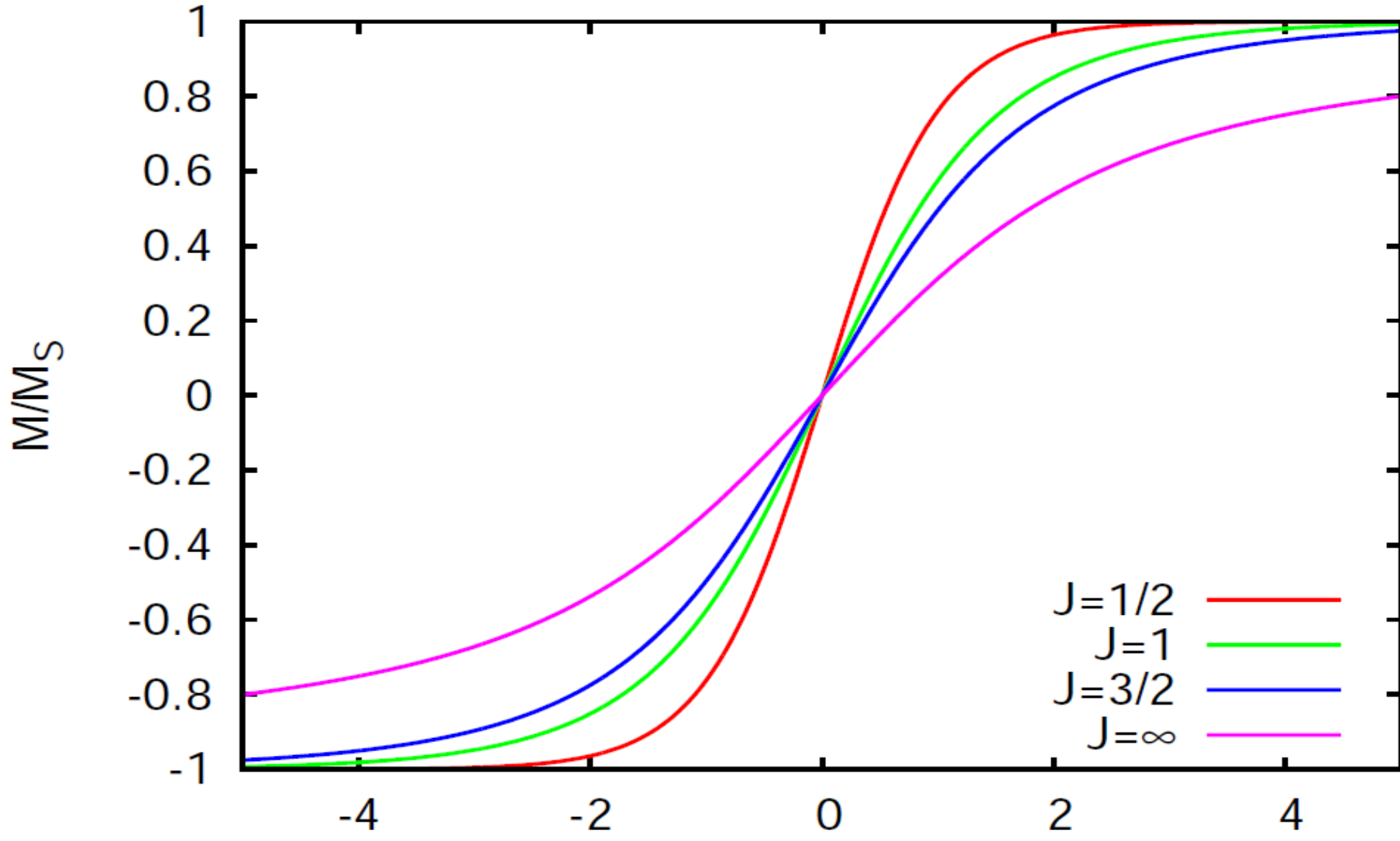
Susceptibilita prvků v závislosti na protonovém čísle



paramagnetické materiály – Langevinova funkce



paramagnetické materiály – Brillouinova funkce



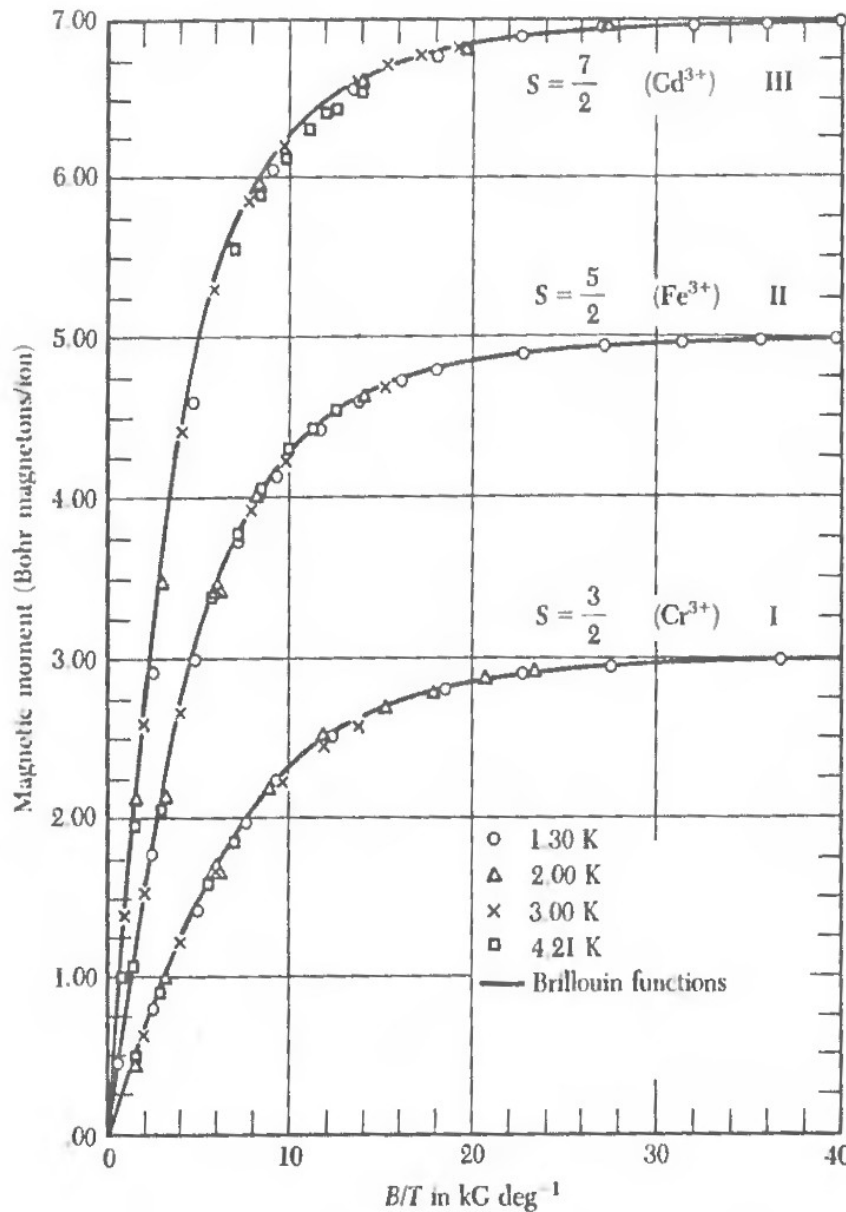
$$B_J(y) = \frac{(2J+1)}{2J} \operatorname{cotgh}\left[\frac{(2J+1)}{2J} y\right] - \frac{1}{2J} \operatorname{cotgh}\left[y/2J\right]$$

Pro $J=1/2$ je $B_{1/2}(y)=\operatorname{arctg}(y)$

Pro $J \rightarrow \infty$ přechází do Langevinovy funkce $B_\infty(y)=L(y)$

Limita pro malá pole a vysoké teploty $B_J(y) \approx y(J+1)/3J$

paramagnetické materiály – závislost magnetizace na teplotě

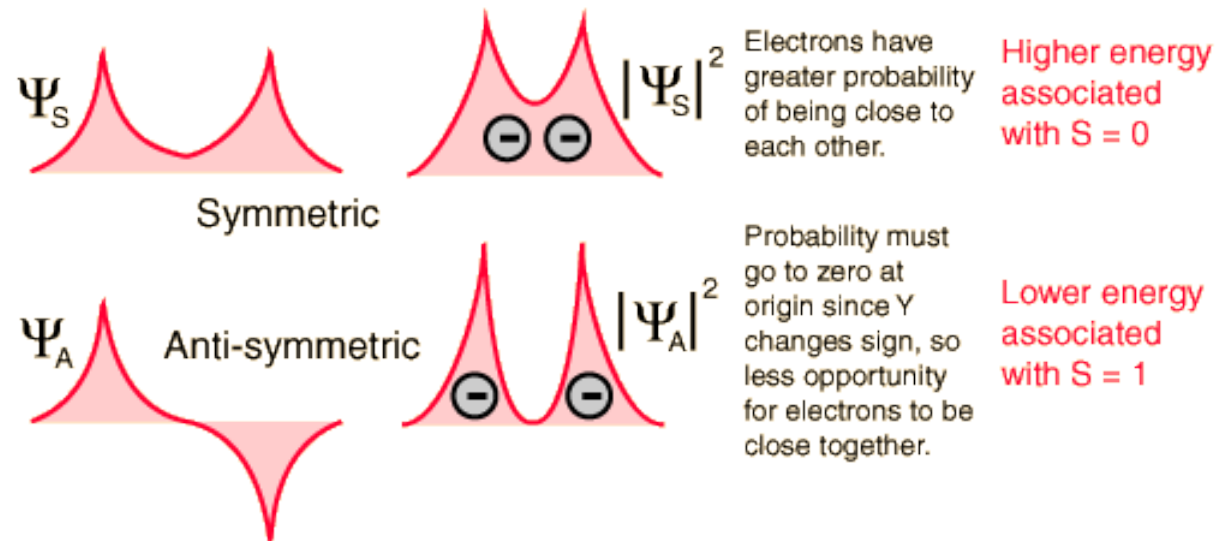
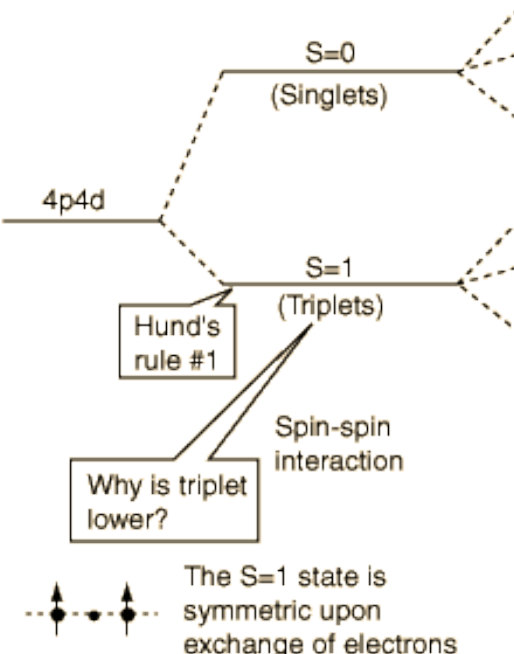


Spojité čára
Brillouinova funkce

Figure 4 Plot of magnetic moment *versus* B/T for spherical samples of (I) potassium chromium alum, (II) ferric ammonium alum, and (III) gadolinium sulfate octahydrate. Over 99.5% magnetic saturation is achieved at 1.3 K and about 50,000 gauss. ($5T$). After W. E. Henry.

Hundova pravidla

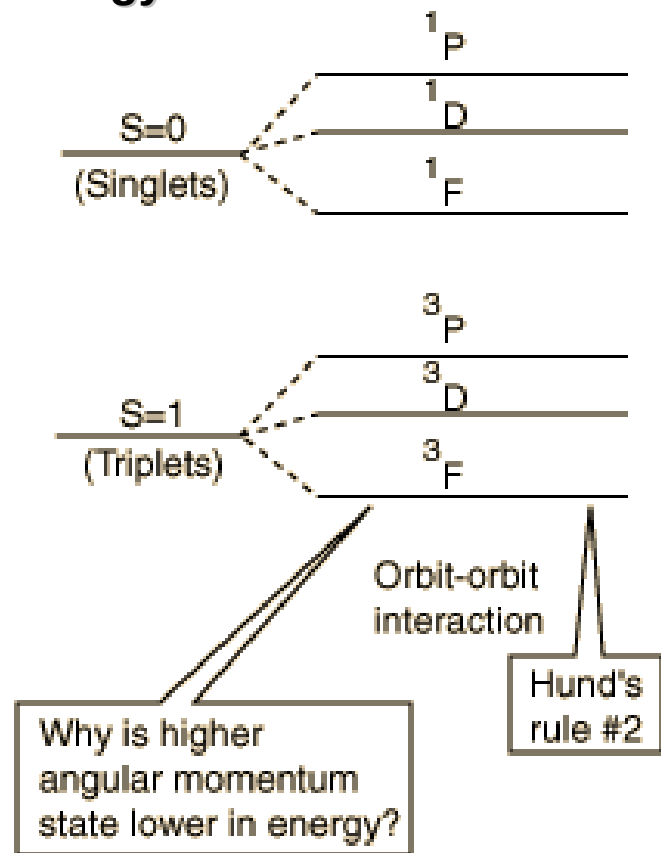
1. The term with the maximum multiplicity lies lowest in energy $\Rightarrow S$ has a maximum possible value



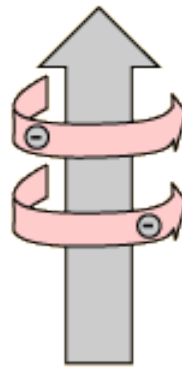
Since $\Psi_{\text{spin}} \Psi_{\text{space}}$ must be anti-symmetric,
then Ψ_{space} must be anti-symmetric to
obey the Pauli exclusion principle.

Hundova pravidla

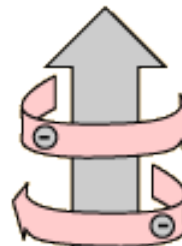
2. For a given multiplicity, the term with the largest value of L lies lowest in energy.



High L , electrons orbiting same direction to add to L value.



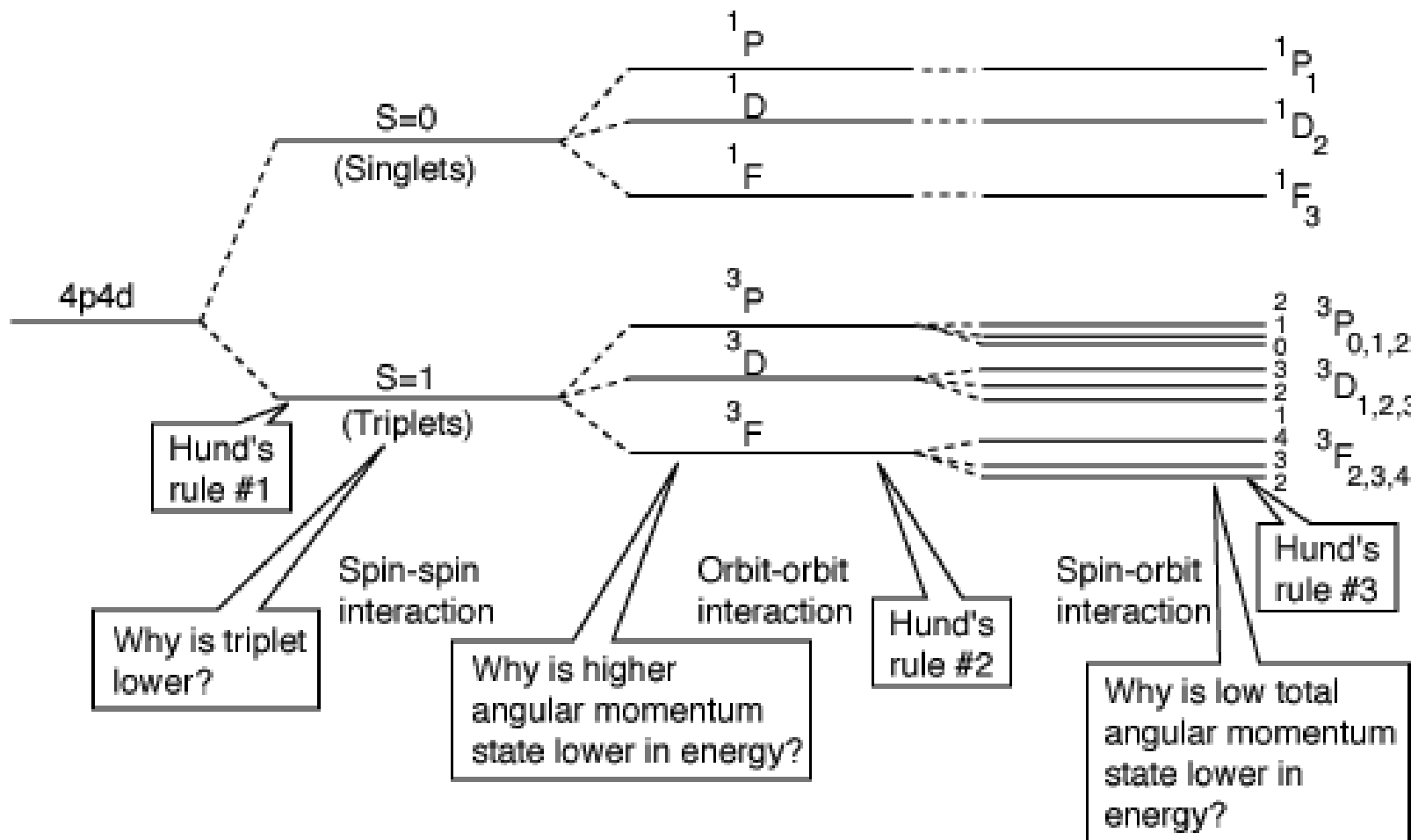
Low L , some electrons orbiting in opposite direction to reduce the L value.



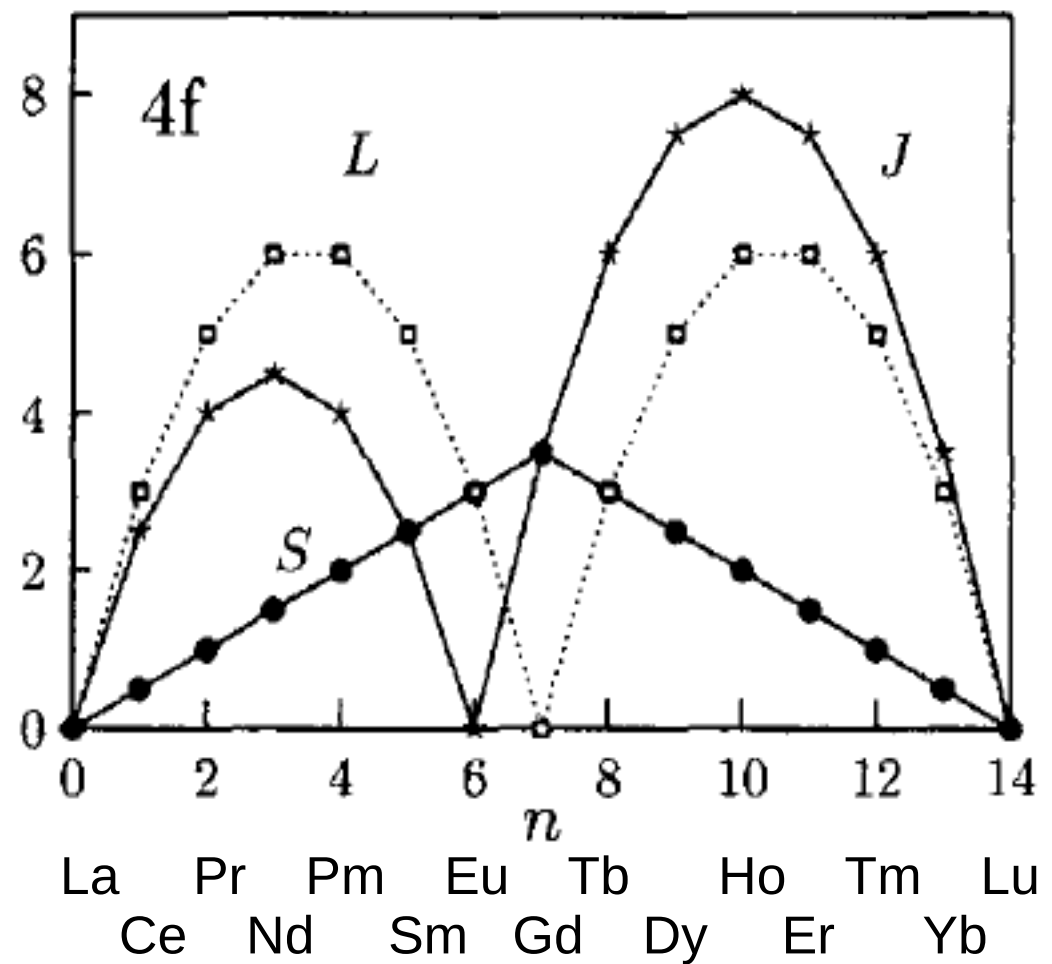
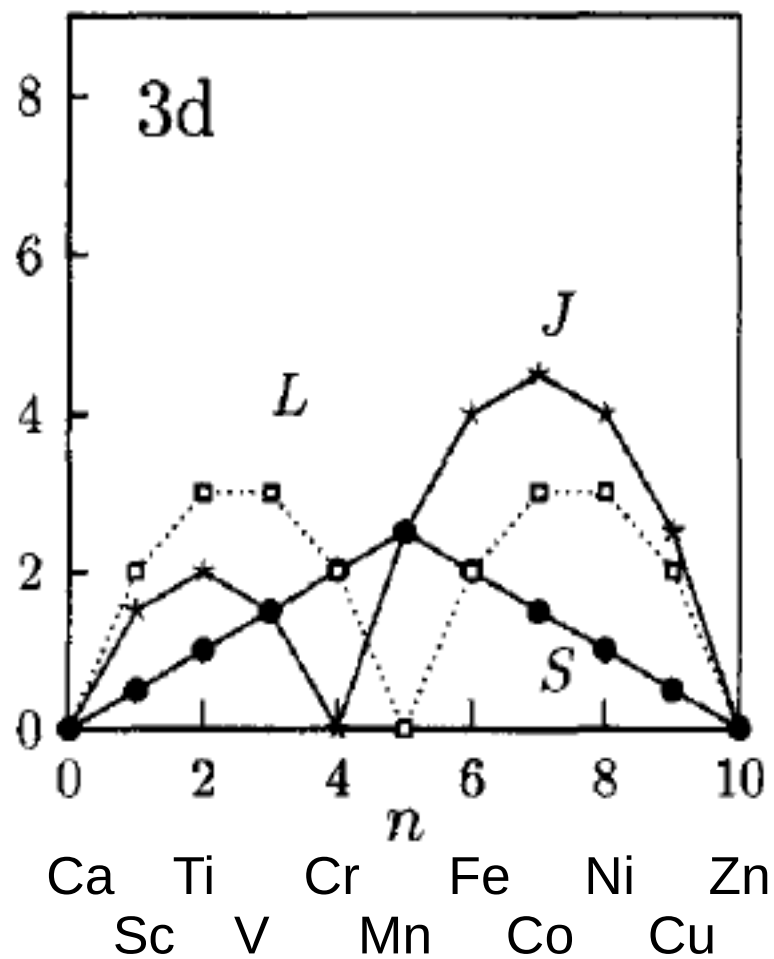
For large L value, some or all of the electrons are orbiting in the same direction. That implies that they can stay a larger distance apart on the average since they could conceivably always be on the opposite side of the nucleus. For low L value, some electrons must orbit in the opposite direction and therefore pass close to each other once per orbit, leading to a smaller average separation of electrons and therefore a higher energy.

Hundova pravidla

3. For atoms with less than half-filled shells, the level with the lowest value of J lies lowest in energy.



Hundova pravidla – 3d a 4f prvky



Hundova pravidla – 4f prvky

Table 2.2 Magnetic ground states for 4f ions using Hund's rules. For each ion, the shell configuration and the predicted values of S , L and J for the ground state are listed. Also shown is the calculated value of $p = \mu_{\text{eff}}/\mu_B = g_J[J(J+1)]^{1/2}$ using these Hund's rules predictions. The next column lists the experimental value p_{exp} and shows very good agreement, except for Sm and Eu. The experimental values are obtained from measurements of the susceptibility of paramagnetic salts at temperatures $k_B T \gg E_{\text{CEF}}$ where E_{CEF} is a crystal field energy.

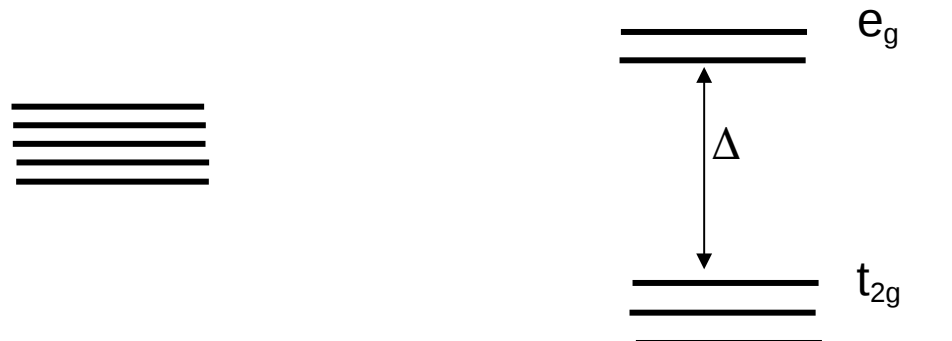
ion	shell	S	L	J	term	p	p_{exp}
Ce ³⁺	4f ¹	$\frac{1}{2}$	3	$\frac{5}{2}$	$^2F_{5/2}$	2.54	2.51
Pr ³⁺	4f ²	1	5	4	3H_4	3.58	3.56
Nd ³⁺	4f ³	$\frac{3}{2}$	6	$\frac{9}{2}$	$^4I_{9/2}$	3.62	3.3–3.7
Pm ³⁺	4f ⁴	2	6	4	5I_4	2.68	–
Sm ³⁺	4f ⁵	$\frac{5}{2}$	5	$\frac{5}{2}$	$^6I_{5/2}$	0.85	1.74
Eu ³⁺	4f ⁶	3	3	0	7F_0	0.0	3.4
Gd ³⁺	4f ⁷	$\frac{7}{2}$	0	$\frac{7}{2}$	$^8S_{7/2}$	7.94	7.98
Tb ³⁺	4f ⁸	3	3	6	7F_6	9.72	9.77
Dy ³⁺	4f ⁹	$\frac{5}{2}$	5	$\frac{15}{2}$	$^6H_{15/2}$	10.63	10.63
Ho ³⁺	4f ¹⁰	2	6	8	5I_8	10.60	10.4
Er ³⁺	4f ¹¹	$\frac{3}{2}$	6	$\frac{15}{2}$	$^4I_{15/2}$	9.59	9.5
Tm ³⁺	4f ¹²	1	5	6	3H_6	7.57	7.61
Yb ³⁺	4f ¹³	$\frac{1}{2}$	3	$\frac{7}{2}$	$^2F_{7/2}$	4.53	4.5
Lu ³⁺	4f ¹⁴	0	0	0	1S_0	0	0

Blundell, Magnetism in solid state, Oxford university press, 2002

Hundova pravidla – 3d prvky

What is the reason for orbital quenching in transition metal ions?

- 3d electrons take part in chemical binding (i.e. FeCl_2 , FeF_3);
- The 3d electrons are subject to strong crystal electric fields (CEF) of the neighbouring ions;
- The CEF lifts the $2L+1$ degeneracy of the d^n - electrons;
- Lifting of degeneracy leads to an energy splitting of the d-shell:

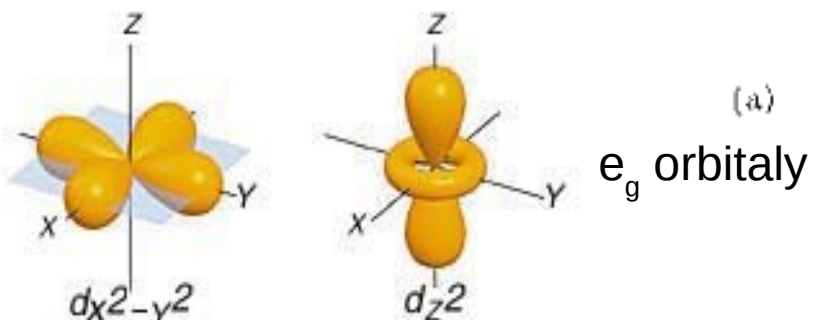
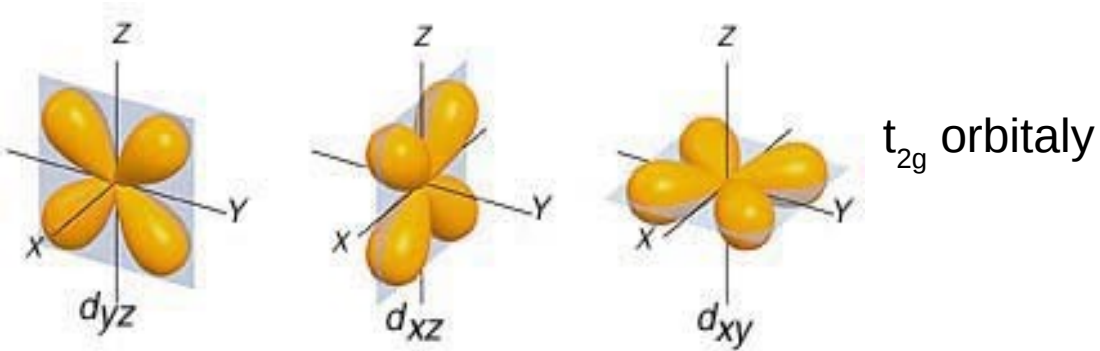


spherical symmetry \Leftrightarrow octahedral symmetry

Δ is the CEF splitting between orbitals of different symmetry; Orbital angular moments of non-degenerate levels have no fixed phase relationship;

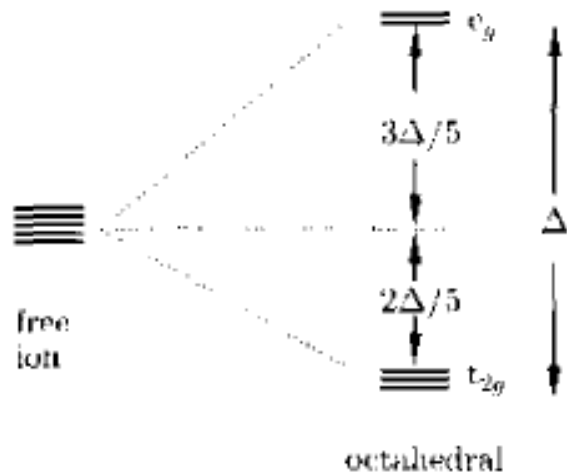
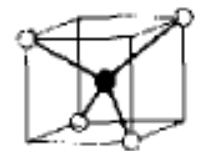
The time average expectation value for the orbital moments is then $\langle L \rangle = 0$; L is not a good quantum number.

Orbitální interakce



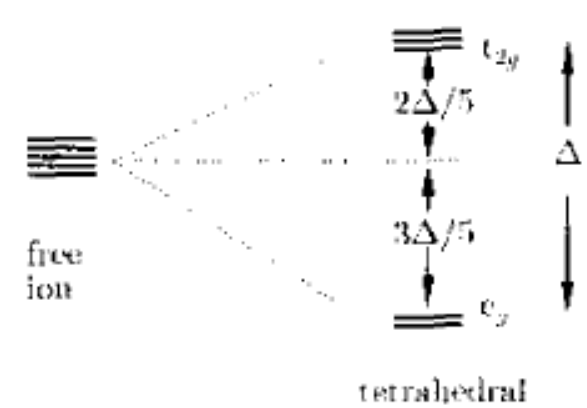
(a)

(b)



free
ion

octahedral



free
ion

tetrahedral

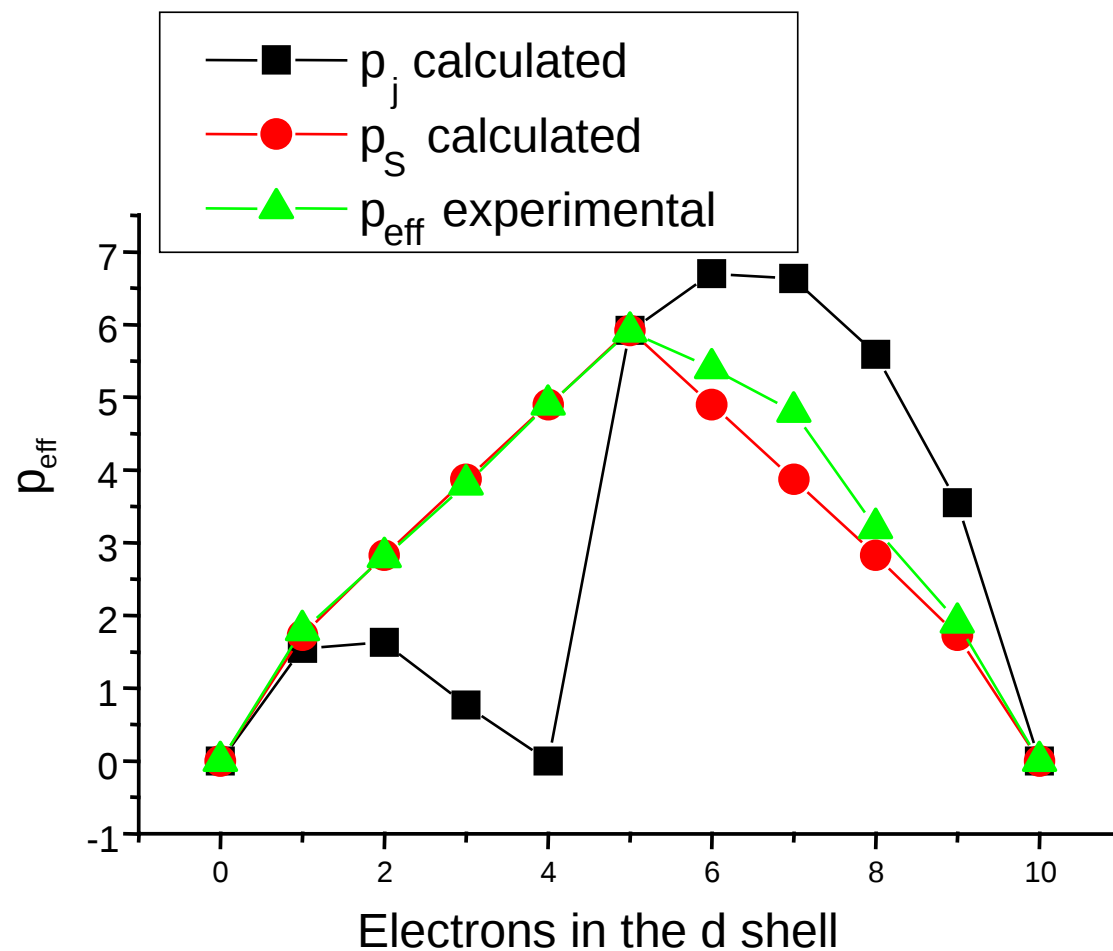
Hundova pravidla – 3d prvky

Table 3.1 Magnetic ground states for 3d ions using Hund's rules. For each ion, the shell configuration and the predicted values of S , L and J for the ground state are listed. Also shown is the calculated value of $p = \mu_{\text{eff}}/\mu_B$ for each ion using Hund's rules predictions. This is given the symbol $p_1 = g_J[J(J+1)]^{1/2}$ and the next column lists the experimental values p_{exp} which are derived from measurements on paramagnetic salts containing the relevant ions. This agrees much better with $p_2 = 2[S(S+1)]^{1/2}$, which assumes orbital quenching, so that $L = 0$, $J = S$ and $g_J = 2$.

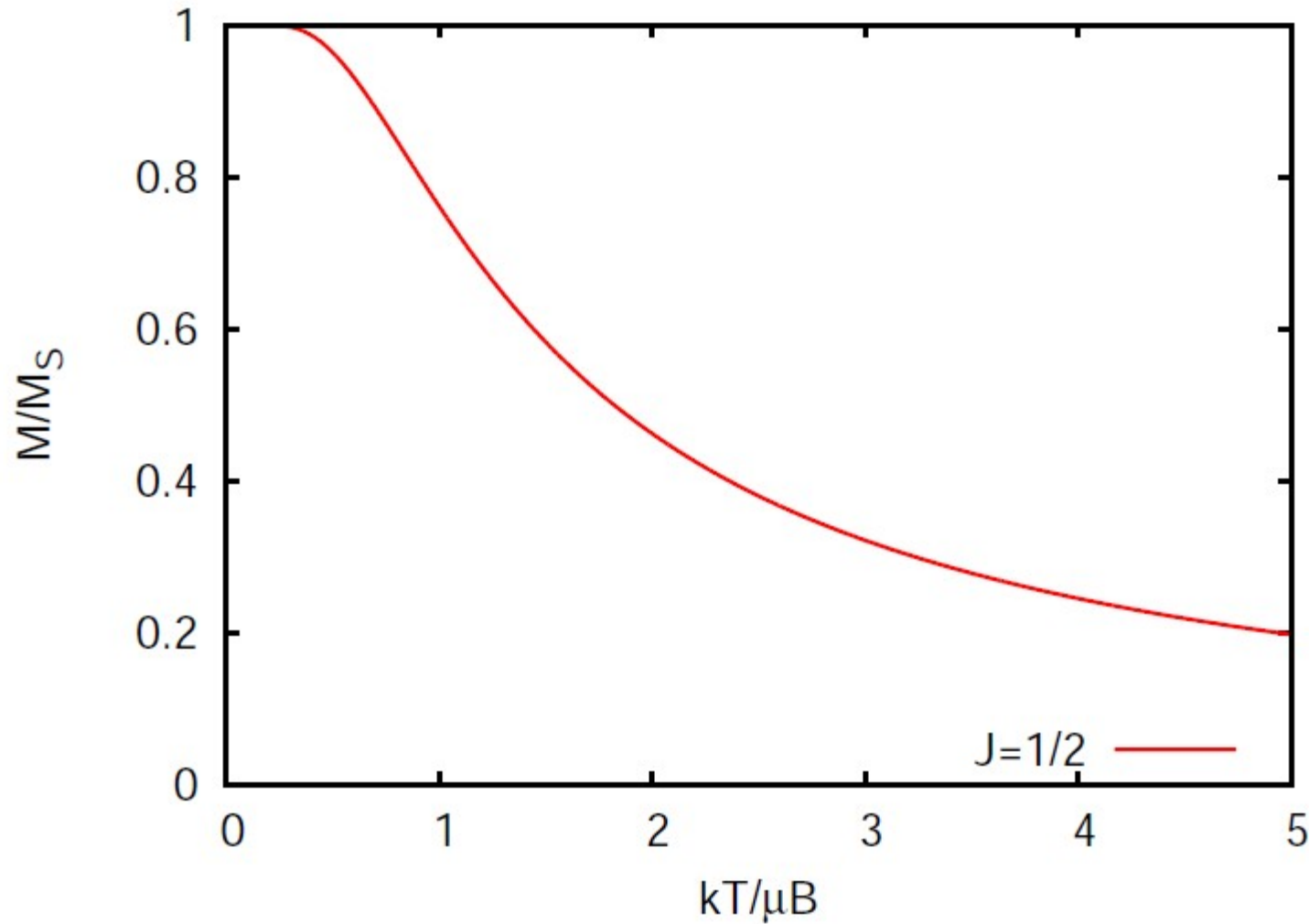
ion	shell	S	L	J	term	p_1	p_{exp}	p_2
Ti ³⁺ , V ⁴⁺	3d ¹	$\frac{1}{2}$	2	$\frac{3}{2}$	$^2D_{3/2}$	1.55	1.70	1.73
V ³⁺	3d ²	1	3	2	3F_2	1.63	2.61	2.83
Cr ³⁺ , V ²⁺	3d ³	$\frac{3}{2}$	3	$\frac{3}{2}$	$^4F_{3/2}$	0.77	3.85	3.87
Mn ³⁺ , Cr ²⁺	3d ⁴	2	2	0	5D_0	0	4.82	4.90
Fe ³⁺ , Mn ²⁺	3d ⁵	$\frac{5}{2}$	0	$\frac{5}{2}$	$^6S_{5/2}$	5.92	5.82	5.92
Fe ²⁺	3d ⁶	2	2	4	5D_4	6.70	5.36	4.90
Co ²⁺	3d ⁷	$\frac{3}{2}$	3	$\frac{9}{2}$	$^4F_{9/2}$	6.63	4.90	3.87
Ni ²⁺	3d ⁸	1	3	4	3F_4	5.59	3.12	2.83
Cu ²⁺	3d ⁹	$\frac{1}{2}$	2	$\frac{5}{2}$	$^2D_{5/2}$	3.55	1.83	1.73
Zn ²⁺	3d ¹⁰	0	0	0	1S_0	0	0	0

Blundell, Magnetism in solid state, Oxford university press, 2002

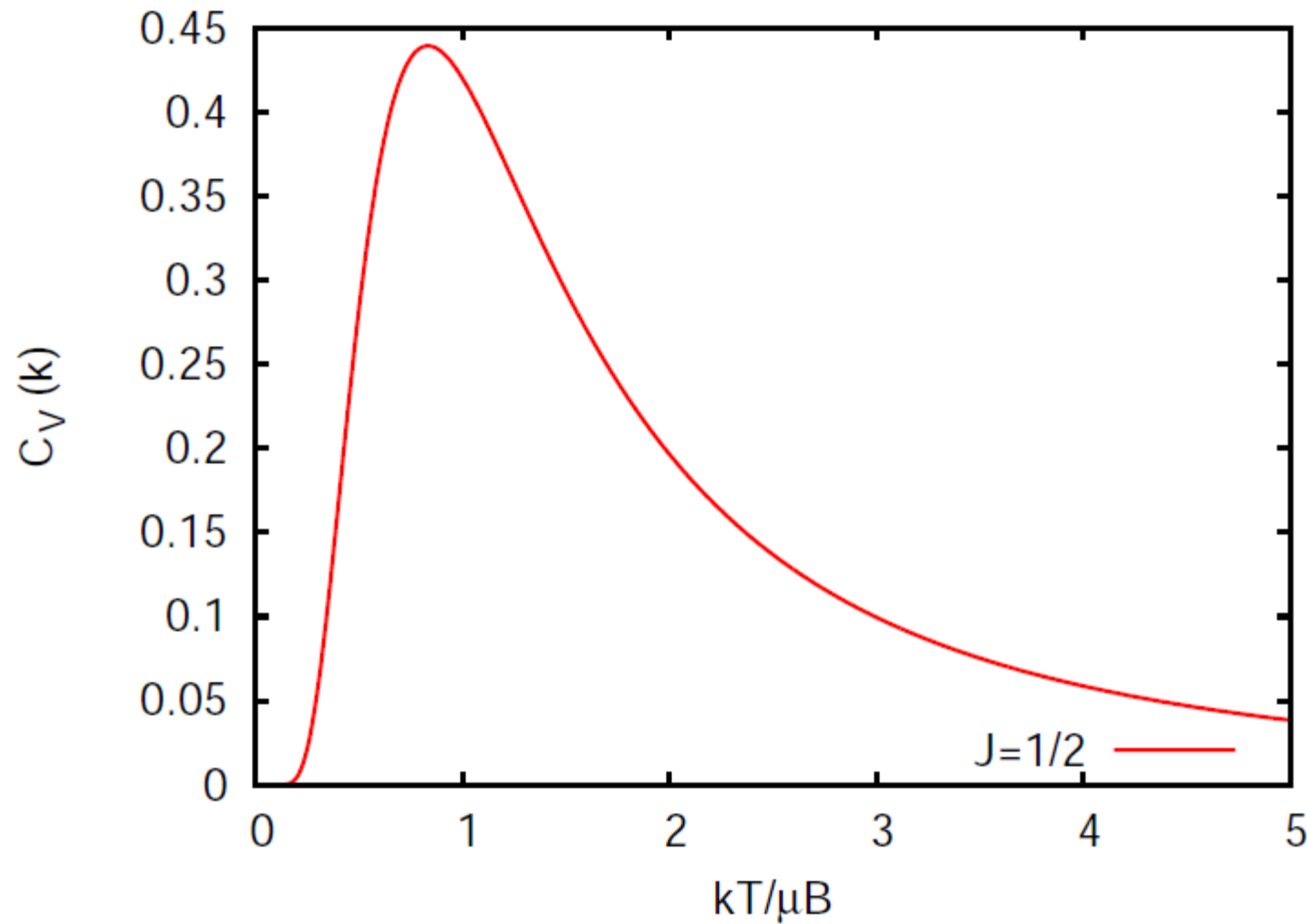
Hundova pravidla – 3d prvky



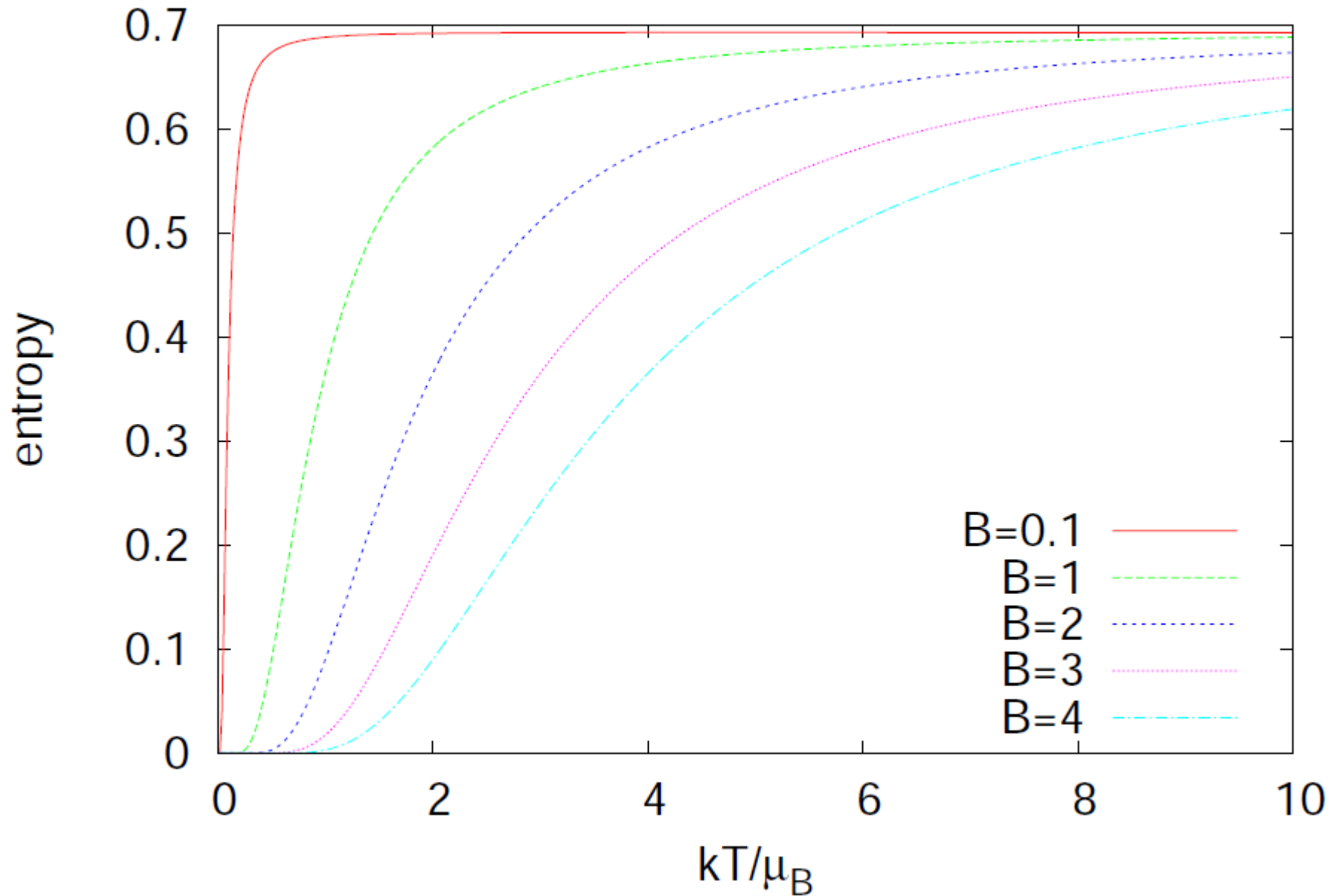
paramagnetické materiály – spin 1/2



paramagnetické materiály – spin $\frac{1}{2}$, měrné teplo



paramagnetické materiály – spin $\frac{1}{2}$, entropie



paramagnetické materiály – entropie, adiabatická demagnetizace

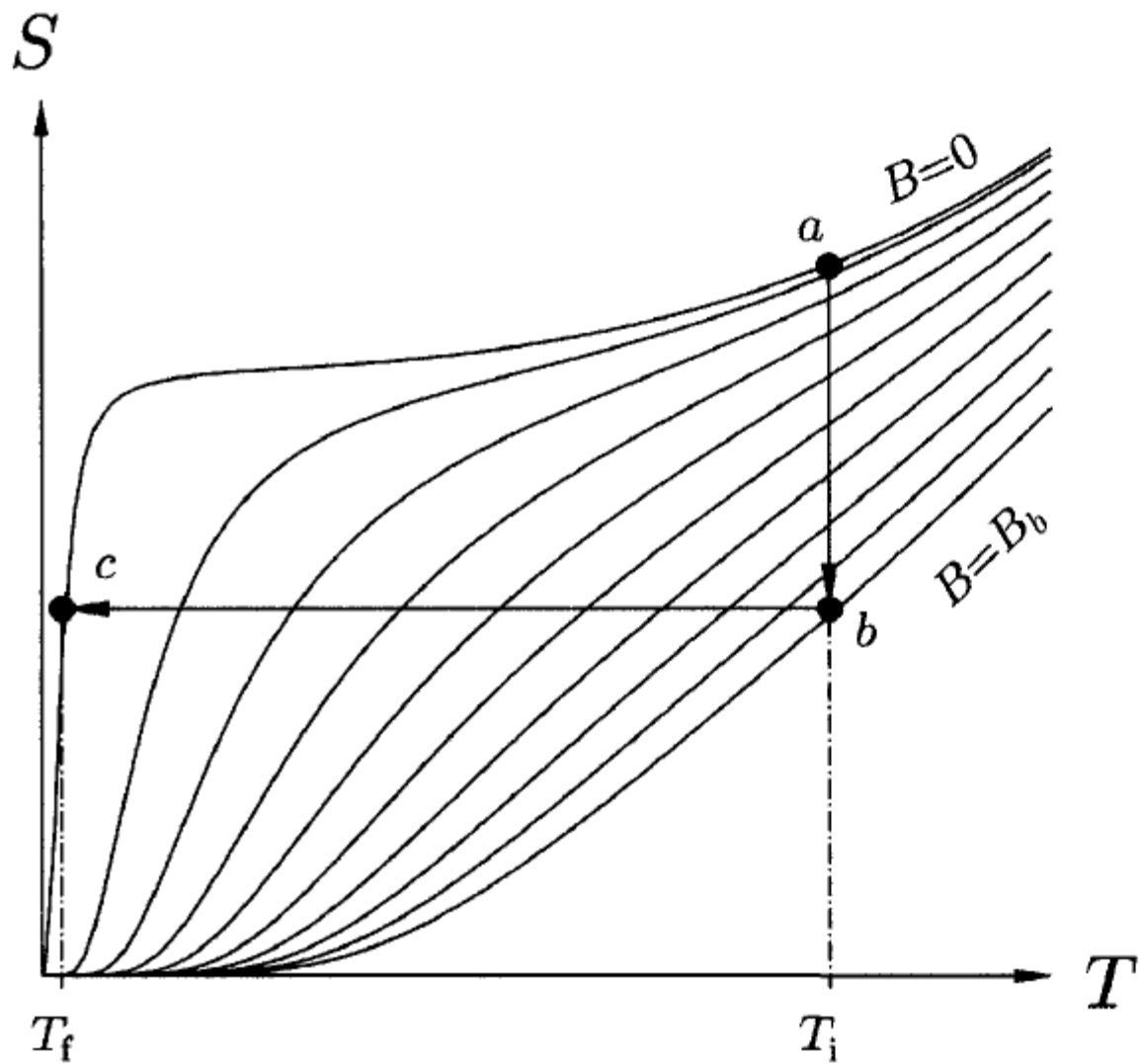


Fig. 2.15 The entropy of a paramagnetic salt as a function of temperature for several different applied magnetic fields between zero and some maximum value which we will call B_b . Magnetic cooling of a paramagnetic salt from temperature T_i to T_f is accomplished as indicated in two steps: first, isothermal magnetization from a to b by increasing the magnetic field from 0 to B_b at constant temperature T_i ; second, adiabatic demagnetization from b to c . The $S(T)$ curves have been calculated assuming $J = \frac{1}{2}$ (see eqn 2.76). A term $\propto T^3$ has been added to these curves to simulate the entropy of the lattice vibrations. The curve for $B = 0$ is actually for B small but non-zero to simulate the effect of a small residual field.

paramagnetické materiály – susceptibilta

	X (10^{-9})	X _{mol} ($10^{-9} \text{ m}^3\text{mol}^{-1}$)	X/p ($10^{-9} \text{ m}^3\text{kg}^{-1}$)
CuSO ₄ .5 H ₂ O			76.7
MnSO ₄ .4 H ₂ O			812
NiSO ₄ .7 H ₂ O			201
Cu			-1.08

paramagnetické materiály – susceptibilita

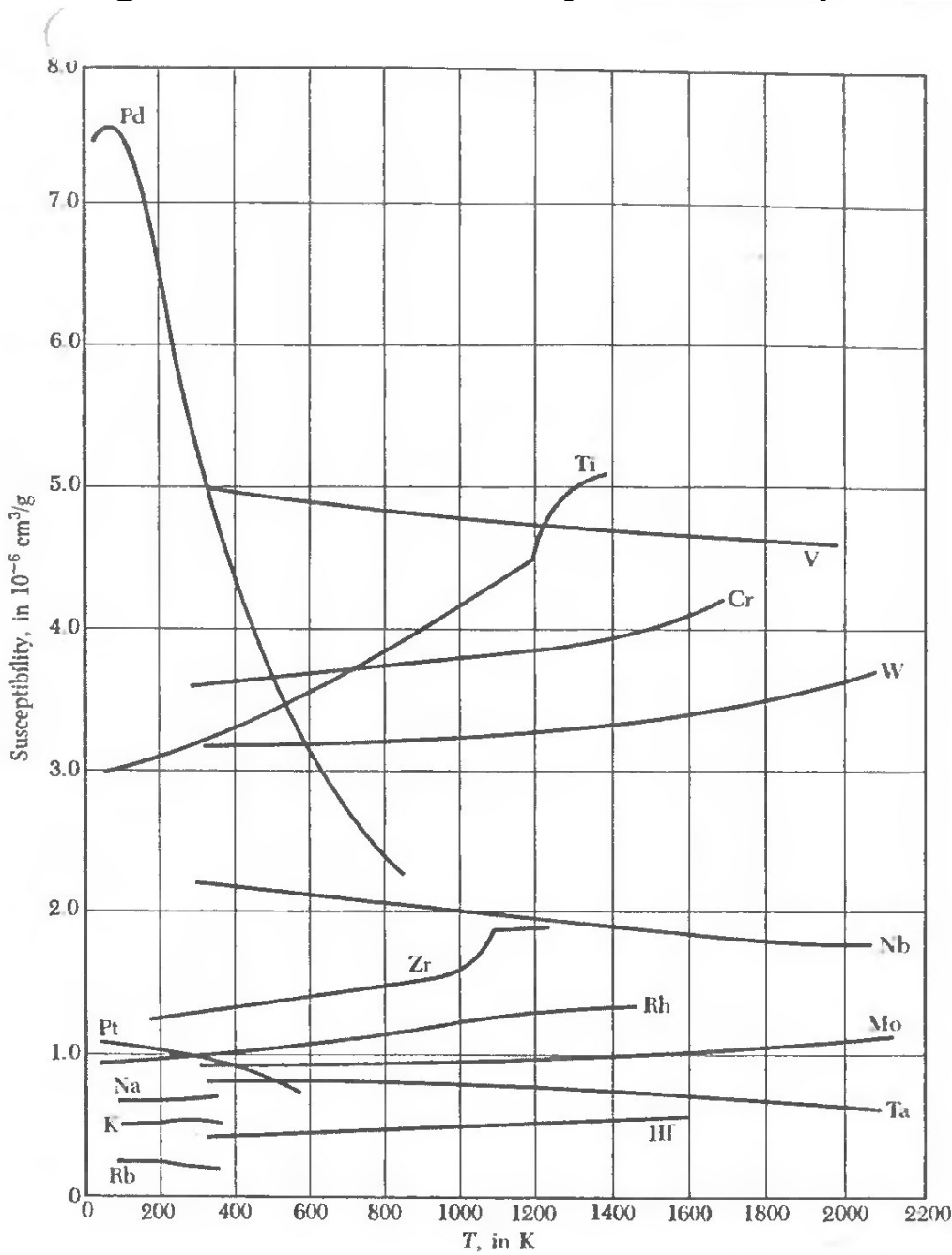
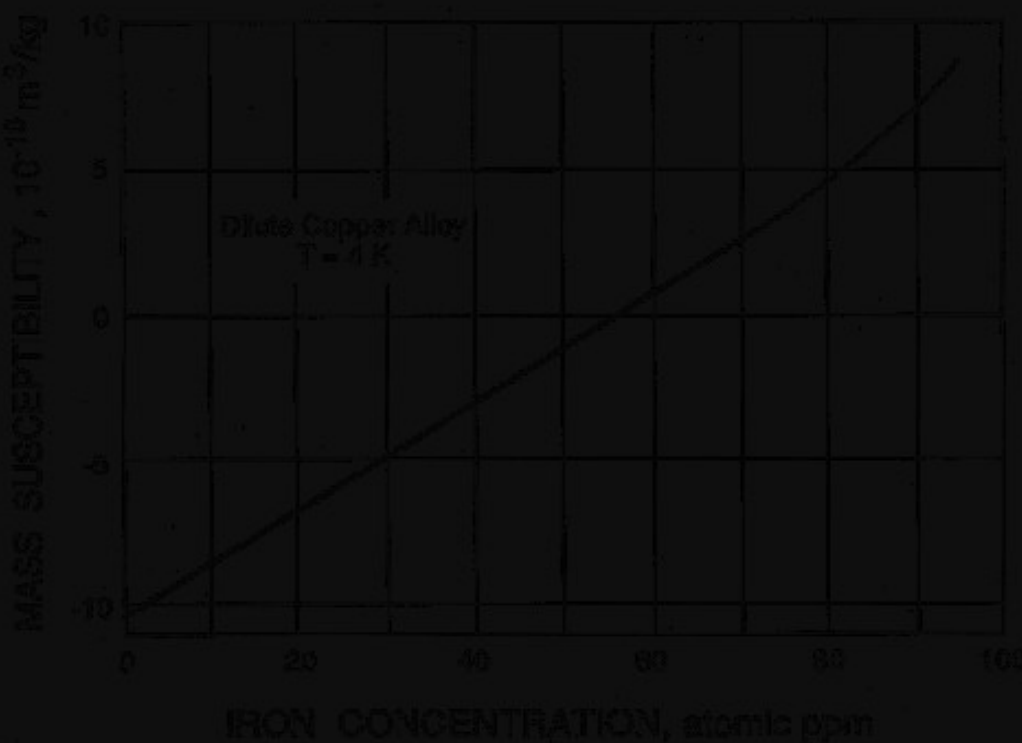


Figure 11 Temperature dependence of the magnetic susceptibility of metals. (Courtesy of C. J. Weissman.)

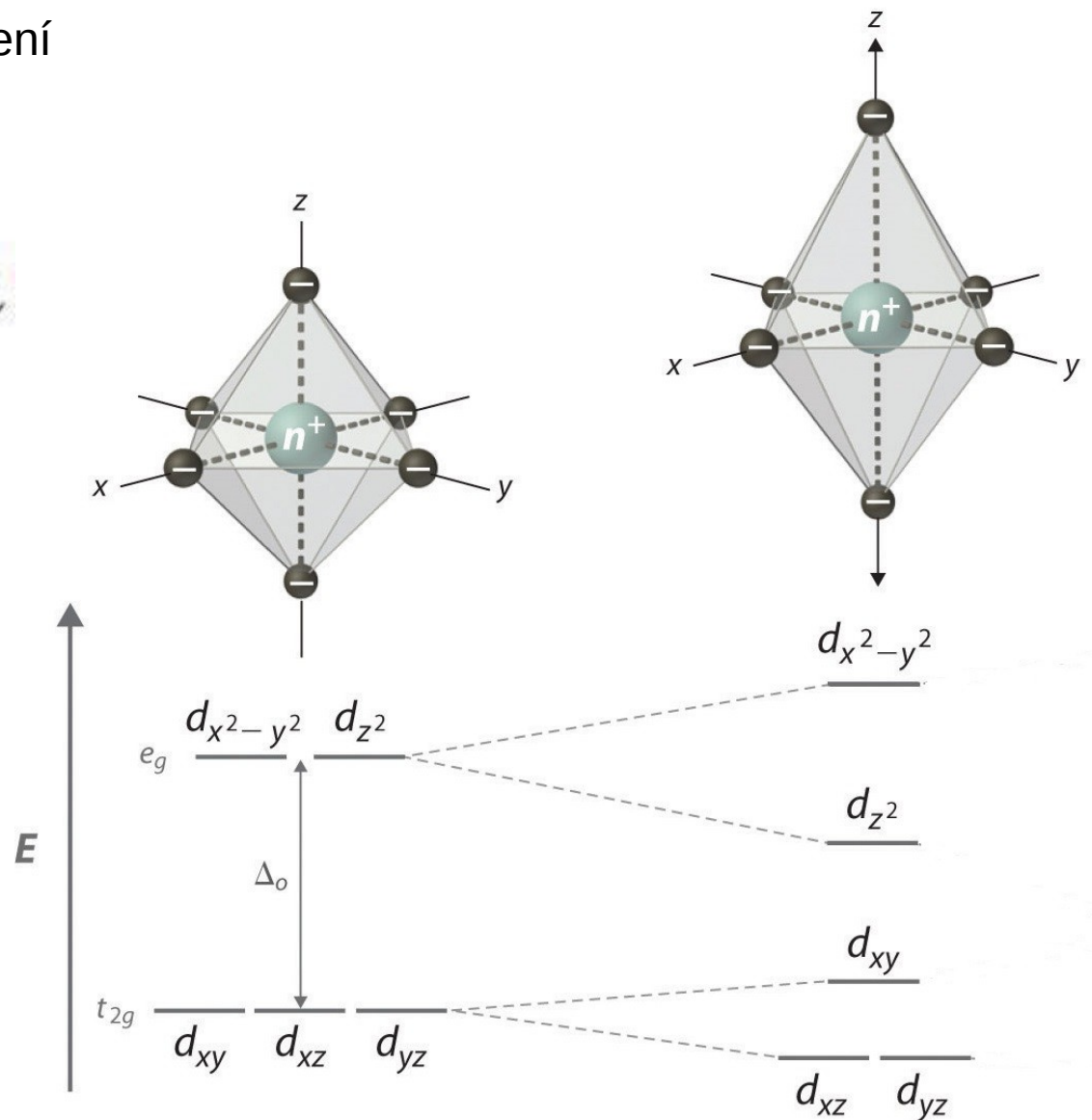
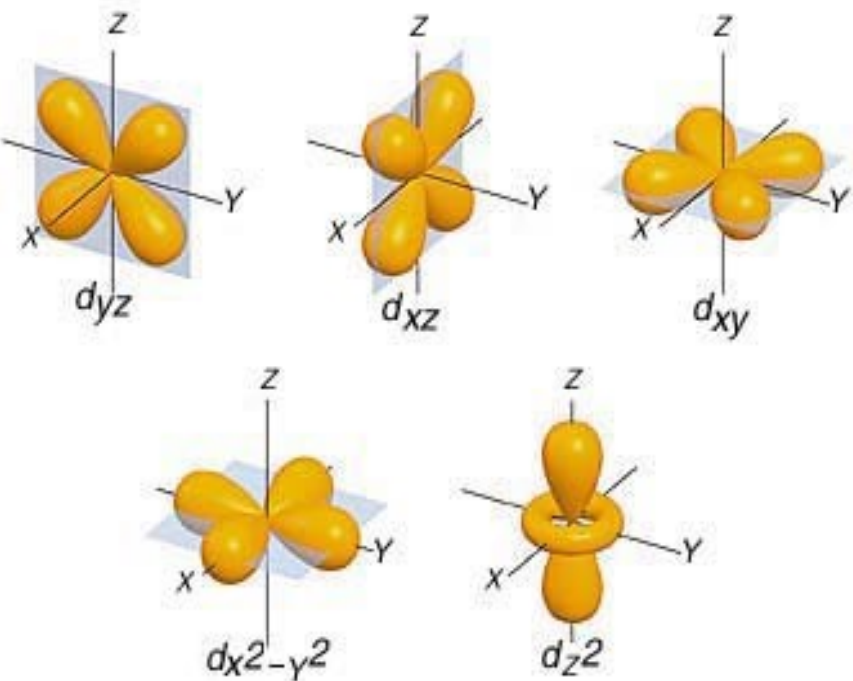
Susceptibilita slitin Cu

ALLOY	Material	Molar Susceptibility, mRb/mole		Volume Susceptibility (3)	
		4 K	273 K	- 30 K	273 K
C16100	Copper Wire	-6.03×10^{-9}	-5.05×10^{-9}	-2.06×10^{-9}	-6.37×10^{-9}
C11100	Electrical Tough Pitch	2.42×10^{-9}	3.64×10^{-9}	2.53×10^{-9}	3.22×10^{-9}
C17200	Nonmagnetic Copper	2.18×10^{-9}	1.87×10^{-9}	1.62×10^{-9}	1.50×10^{-9}
C17200	Beryllium Copper (B20)	1.64×10^{-9}	1.14×10^{-9}	1.20×10^{-9}	1.40×10^{-9}
C22000	Commercial Bronze	2.67×10^{-9}	-6.40×10^{-9}	7.60×10^{-9}	-5.64×10^{-9}
C28000	Free Cutting Bronze	-9.05×10^{-9}	1.27×10^{-9}	-1.71×10^{-9}	1.13×10^{-9}



Orbitální interakce

Jahn-Tellerovo rozštěpení



Výměnná interakce – přímá výměna

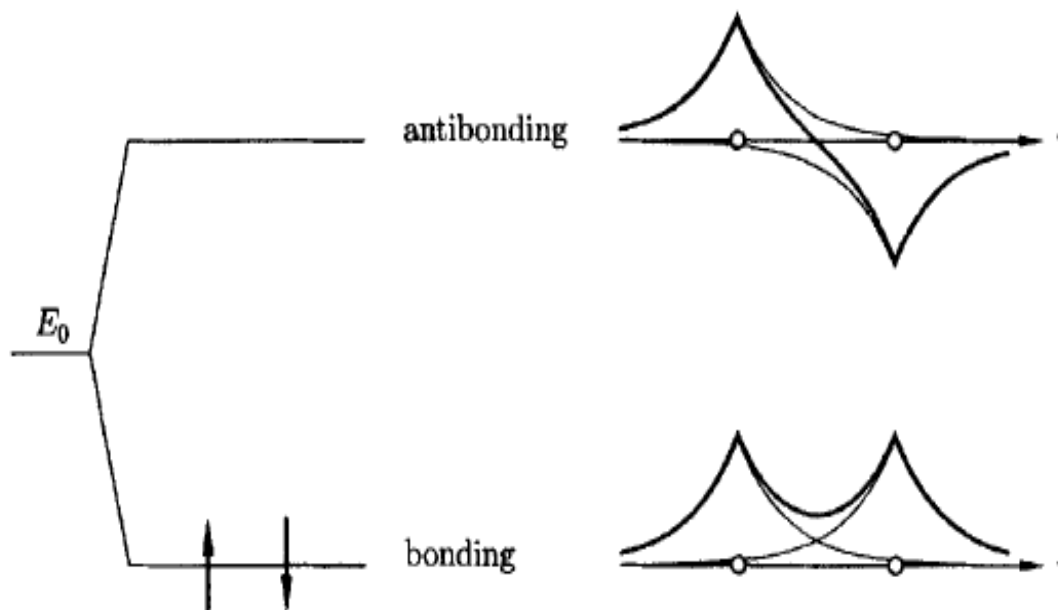
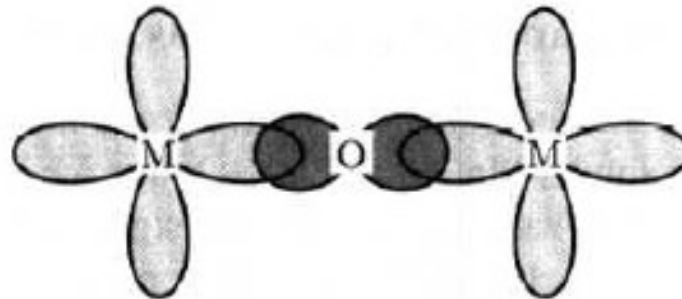
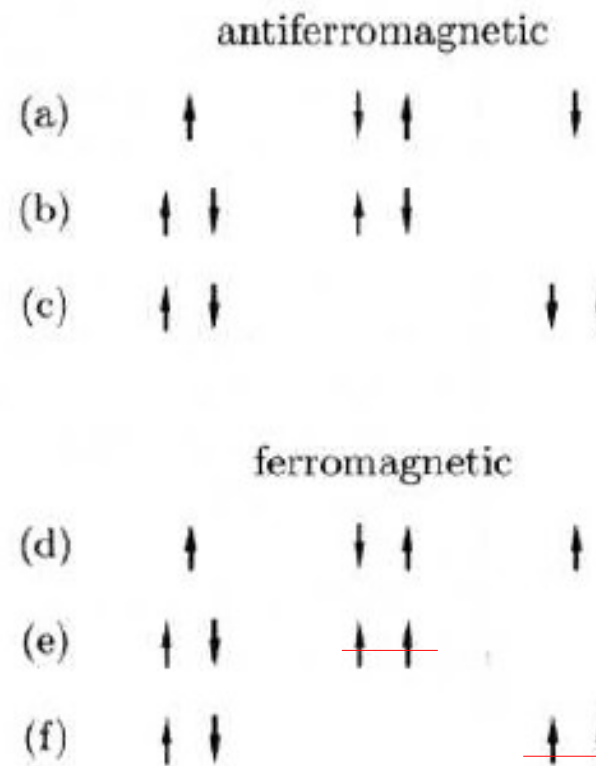
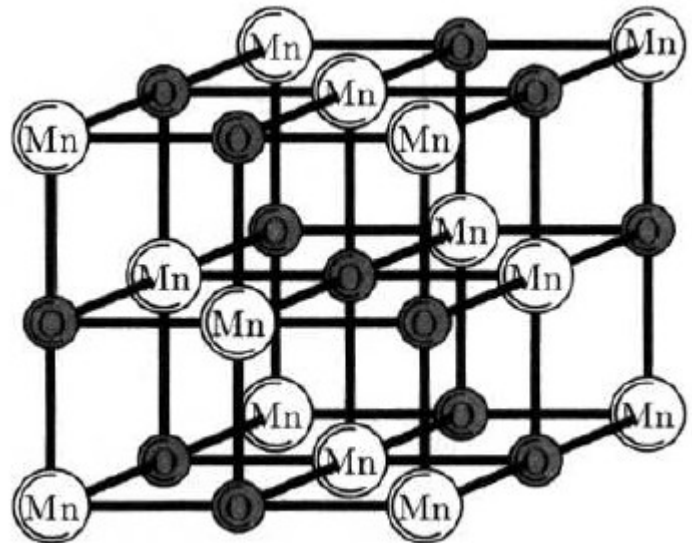
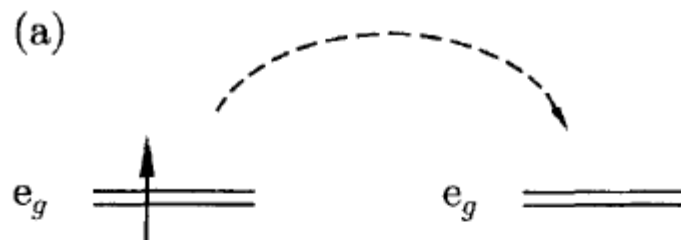


Fig. 4.1 Molecular orbitals for a diatomic molecule. The bonding orbital, which corresponds to the sum of the two atomic orbitals (symmetric under exchange, as far as the spatial part of the wave function is concerned), is of lower energy than the antibonding orbital, which corresponds to the difference of the two atomic orbitals (antisymmetric under exchange). This therefore favours a singlet ground state in which two electrons fill the bonding state and the antibonding state is empty. This diagram is appropriate for the hydrogen molecule H_2 which has a lower energy than that of two isolated H atoms (E_0). Note that the diatomic form of helium, He_2 , does not form because the four electrons from two He atoms would fill both the bonding and antibonding orbitals, corresponding to no net energy saving in comparison with two isolated He atoms.

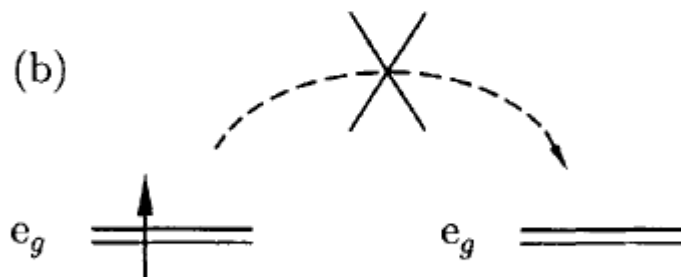
Výměnná interakce – supervýměna



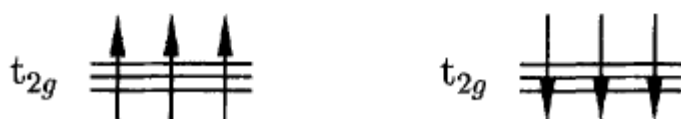
Výměnná interakce – dvojitá výměna



feromagnetické uspořádání -
elektricky vodivé



paramagnetické uspořádání -
elektricky nevodivé



Mn^{3+} $3d^4$

Kolosální magnetorezistence

Feromagnetické prvky

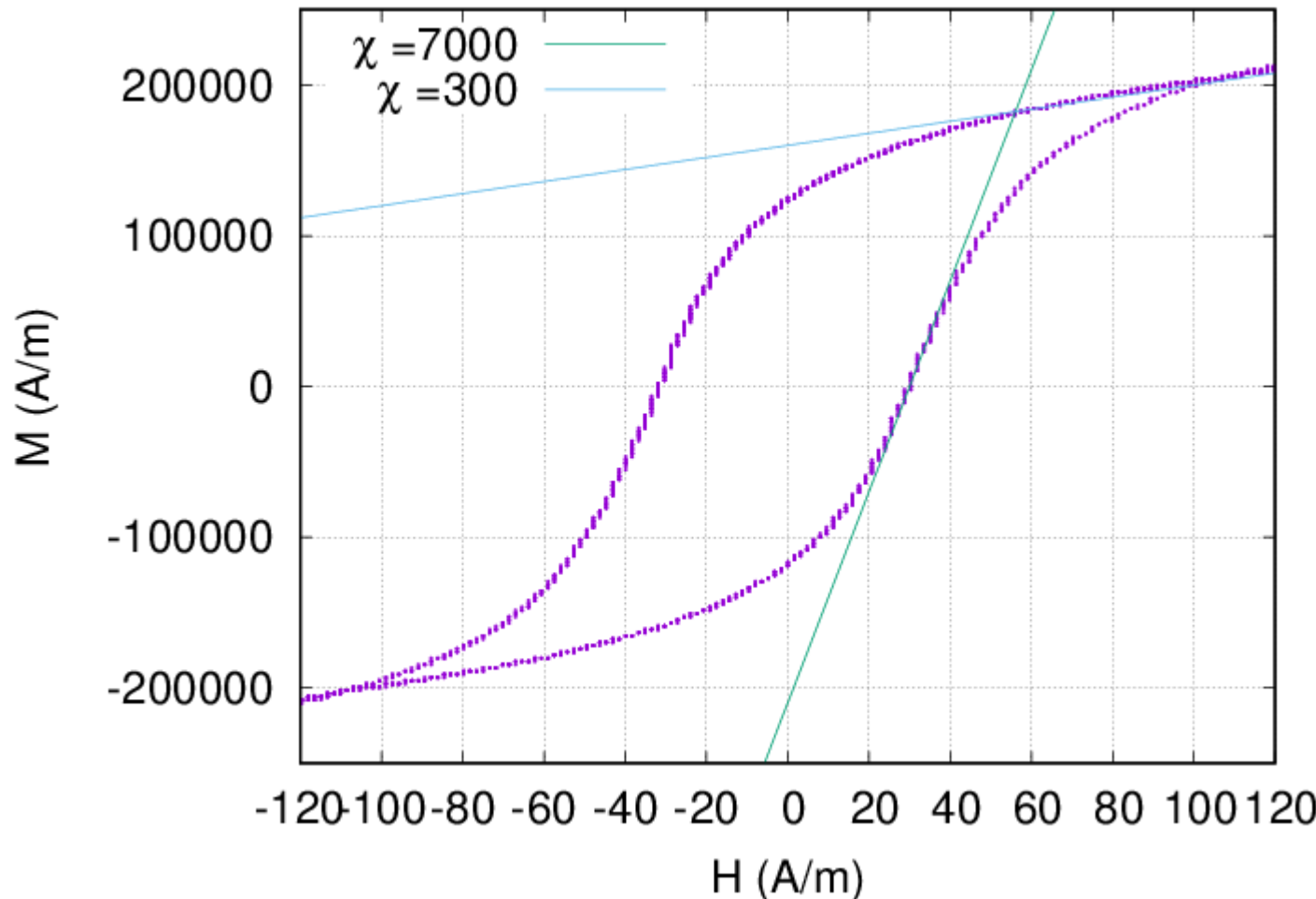
	T_c (K)	$M_n / 300K$ (T)	$M_n / 0K$ (T)
Fe	1040	2.149	2.20
Co	1400	1.798	1.82
Ni	630	0.609	0.64
Gd	290		2.49
Tb	223		
Dy	87		3.8
Ho	20		
Er	20		
Tm	38		

Feromagnetické sloučeniny

	T_c (K)	M_n (μ_B)	M_n (T) / 0K
MnSb	587	7.5	
EuO	70	6.9	2.40
EuS	16.5	6.9	1.49
MnAs	318		1.09
MnBi	670		0.85
GdCl ₂	2.2		0.69

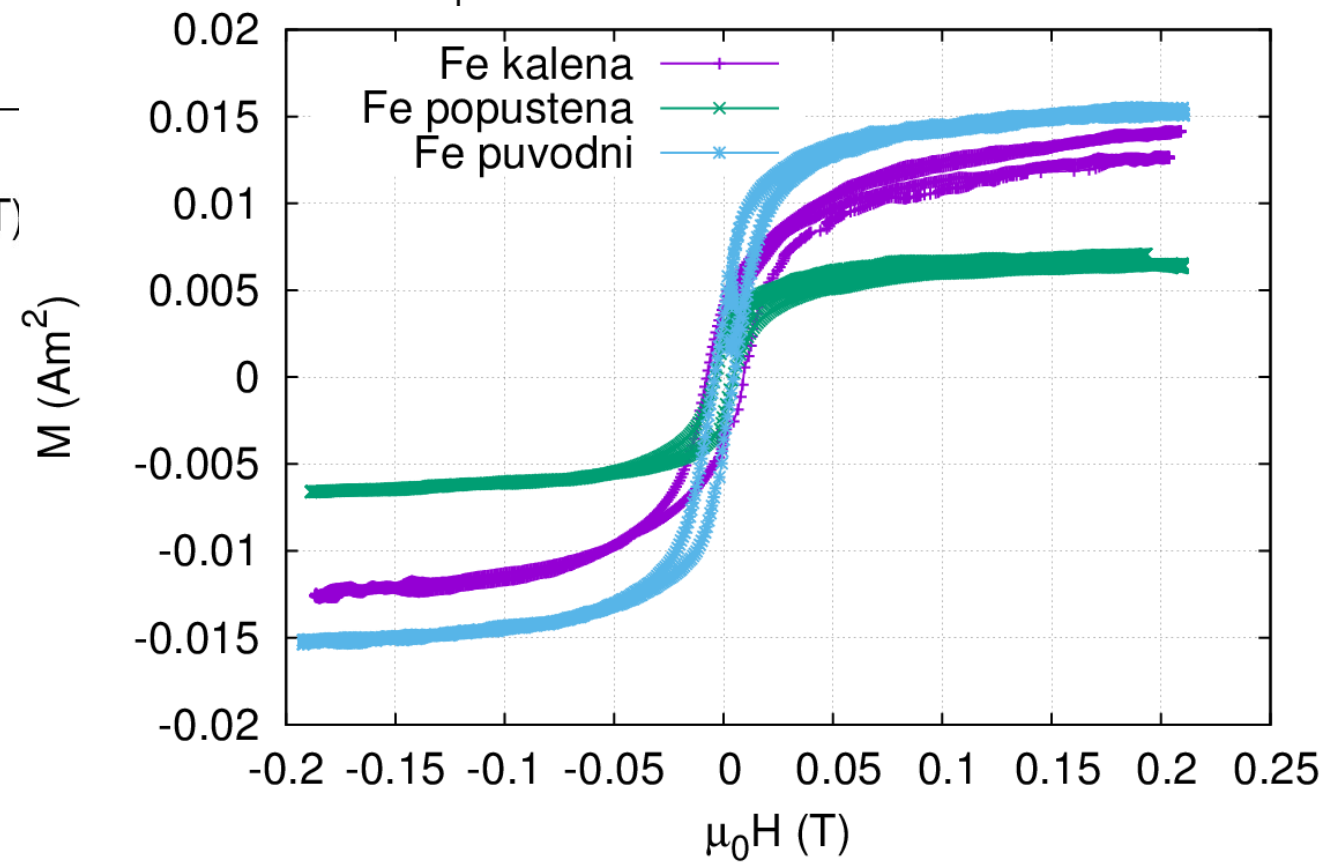
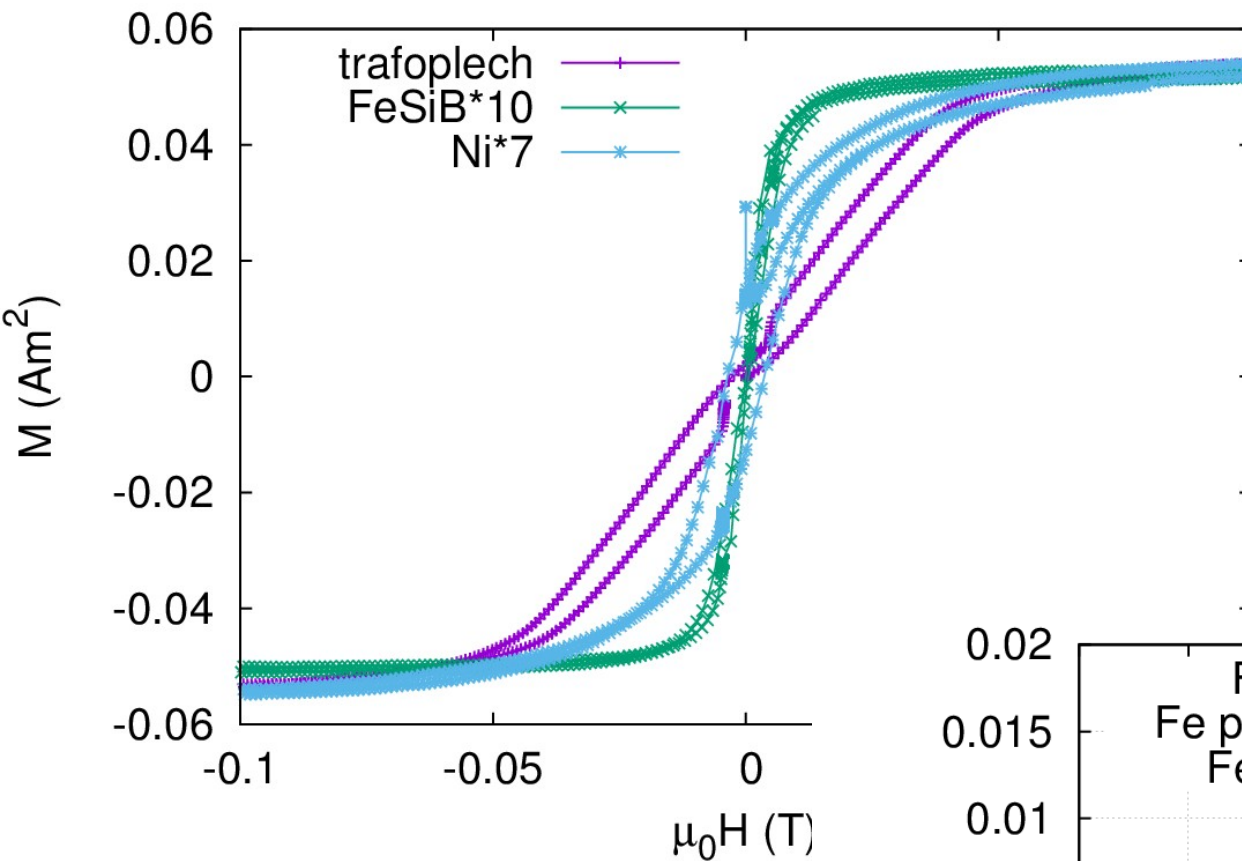
Hysterezní smyčka

Fyz.praktikum 2



Feritové jádro PRAMET Šumperk, n.p.

Hysterezní smyčka



Feromagnetické materiály

TABLE W17.2 Technologically Important Magnetic Materials

Material	Magnetically Hard or Soft	Applications
Metals		
Steels (alloyed with W, Cr, etc.)	Hard	Permanent magnets
Fe particles (oxide-coated)	Hard	Magnetic recording media
Fe _x Ni _{1-x} alloys: 78 Permalloy, Fe _{0.22} Ni _{0.78} ; Supermalloy, Fe _{0.16} Ni _{0.79} Mo _{0.05} ; Invar, Fe _{0.65} Ni _{0.35}	Soft	Electromagnetic devices, magnetic recording heads, precision instruments
Mumetal: ≈ Fe _{0.18} Ni _{0.77} Cu _{0.05}	Soft	Magnetic shielding, transformer cores
Co alloys (CoCr, etc.)	Hard	Magnetic recording media
Fe _{1-x} Si _x	Soft	Transformer cores
Fe:Si:Al alloys: Sendust, ^a 85Fe10Si5Al	Soft	Magnetic recording heads
Alnico alloys: Alnico 5, ^a 51Fe14Ni8Al24Co3Cu	Hard	Permanent magnets
Amorphous rare earth-transition metal alloys	Soft	Magneto-optical recording media
Amorphous Fe:B:Si:C alloys	Soft	Magnetostrictive elements
Intermetallic compounds		
SmCo ₅ and Sm ₂ Co ₁₇	Hard	Permanent magnets
Nd ₂ Fe ₁₄ B	Hard	Permanent magnets
TbFe ₂ and (Tb _{0.3} Dy _{0.7})Fe ₂ (Terfenol-D)	Soft	Magnetostrictive elements
Ceramic compounds		
γ-Fe ₂ O ₃	Hard	Magnetic recording media
CrO ₂	Hard	Magnetic recording media
Mn _{1-x} Zn _x Fe ₂ O ₄	Soft	Magnetic recording heads
Y ₃ Fe ₅ O ₁₂ (YIG)	Soft	Microwave technology
BaO·6Fe ₂ O ₃ or SrO·6Fe ₂ O ₃ (BaFe ₁₂ O ₁₉ , SrFe ₁₂ O ₁₉)	Hard	Permanent magnets, magnetic recording media

^aComposition given in weight percent.

Gersten, Smith,
The physics
and chemistry
of materials,
Wiley 2001.

Feromagnetické materiály – permanentní magnety

TABLE W17.3 Properties of Permanent-Magnet Materials

Material	$(BH)_{\max}$ (kJ/m ³) ^a	B_r (T)	H'_c (kA/m)	T_c (K)
Transition Metal Alloys				
Alnico 5 ^c : (51Fe, 14Ni, 8Al, 24Co, 3Cu)	35.8	1.25	43.8	1120
Steels ^c				
Cobalt steel (35Co, 0.7C, 4Cr, 5W, bal. Fe)	7.7	0.95	19.1	
Tungsten steel (5W, 0.3Mn, 0.7C, bal. Fe)	2.5	1.03	5.6	
Rare Earth–Transition Metal Intermetallic Compounds				
Nd–Fe–B ^d	200–380	1.0–1.4	700–1000	580
SmCo ₅ ^e	130–180	0.8–0.9	600–670	990
Sm(Co,Fe,Cu,Zr) ₇ ^e	200–240	0.95–1.15	600–900	1070
Ceramics				
BaO·6Fe ₂ O ₃ ^d	28	0.4	250	720

^aNote that 1 kJ/m³ = 1 kA·T/m.

^bThe quantity H'_c is the coercive field corresponding to $B = 0$.

^cData from D. R. Lide and H. P. R. Frederikse, eds., *CRC Handbook of Chemistry and Physics*, CRC Press, Boca Raton, Fla., 1994, pp. 12–113. The alloy composition is given in weight percent. See the Handbook for methods of fabrication.

^dCommercial material from Magnet Sales & Manufacturing Catalog.

^eData from K. H. J. Buschow, *Rep. Prog. Phys.*, **54**, 1123 (1991). Sm(Co,Fe,Cu,Zr)₇ is a two-phase material which can be thought of as a composite of SmCo₅- and Sm₂Co₁₇-type phases.

Feromagnetické materiály – železné slitiny

TABLE W17.4 Magnetic Properties of Pure Fe and Some Magnetically Soft Fe Alloys and Electrical Steels at Room Temperature

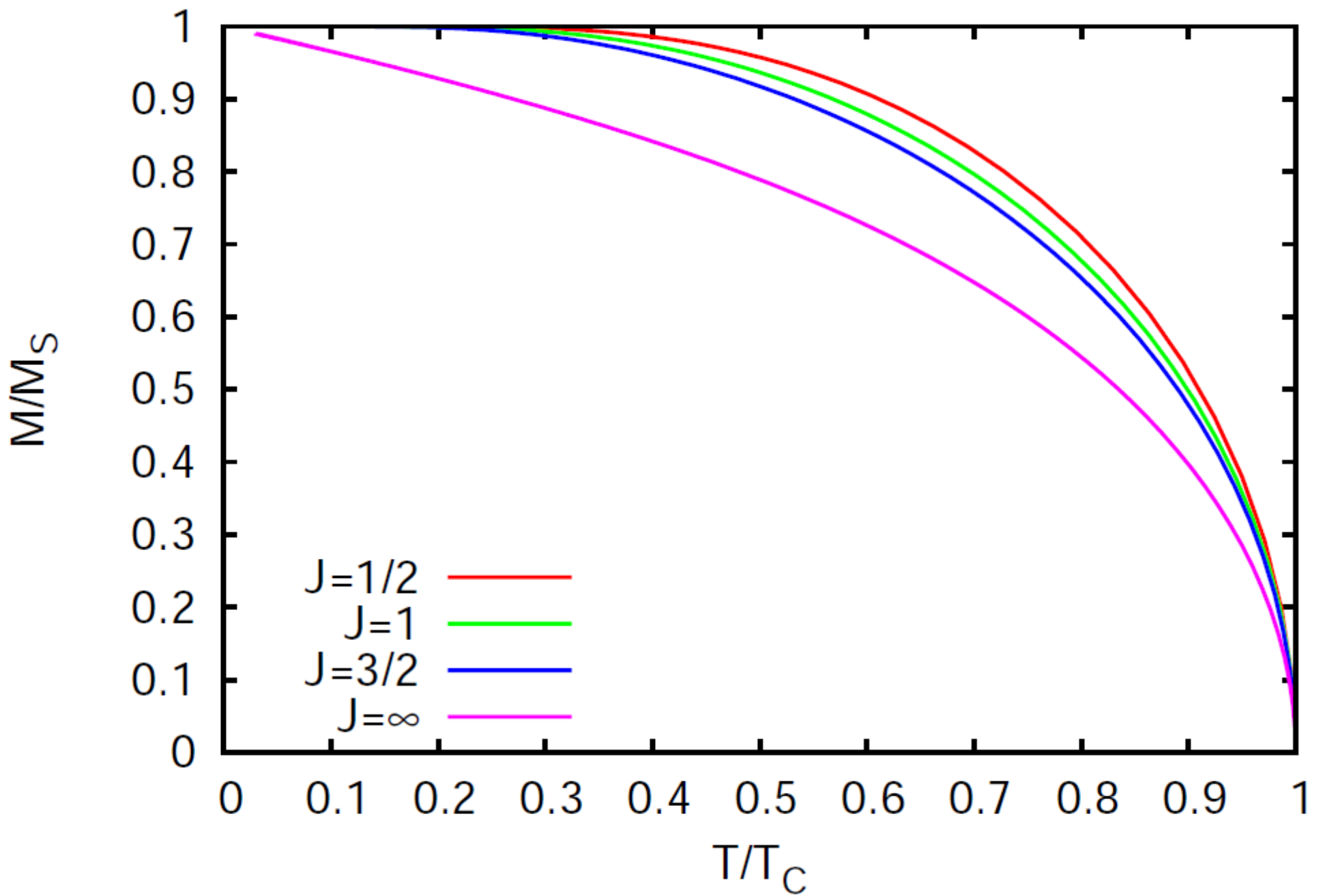
Alloy ^a	$\mu_r(\text{max})^b$	H_c (A/m)	M_s (10^3 kA/m)
“Pure” α -Fe ($\approx 99\%$)	$\approx 10^3$	80	1.71
Pure α -Fe ($\approx 99.99\%$)	2×10^5	0.8	1.71
78 Permalloy (78Ni, 22Fe)	$\approx 10^5$	4	0.86
Supermalloy (79Ni, 16Fe, 5Mo)	$\approx 10^6$	0.16	0.63
Mumetal (77Ni, 18Fe, 5Cu)	2.4×10^5	2	≈ 0.5
Hipernik (50Ni, 50Fe)	7×10^4	4	1.27
Silicon-iron (97Fe, 3Si) (oriented)	4×10^4	8	1.6
Amorphous Fe ₈₀ B ₁₁ Si ₉	—	2	1.27

Source: Data for Fe₈₀B₁₁Si₉ from N. Cristofaro, *Mater. Res. Soc. Bull.*, May 1998, p. 50; remaining data from A. Chikazumi, *Physics of Magnetism*, Wiley, New York, 1964, p. 494.

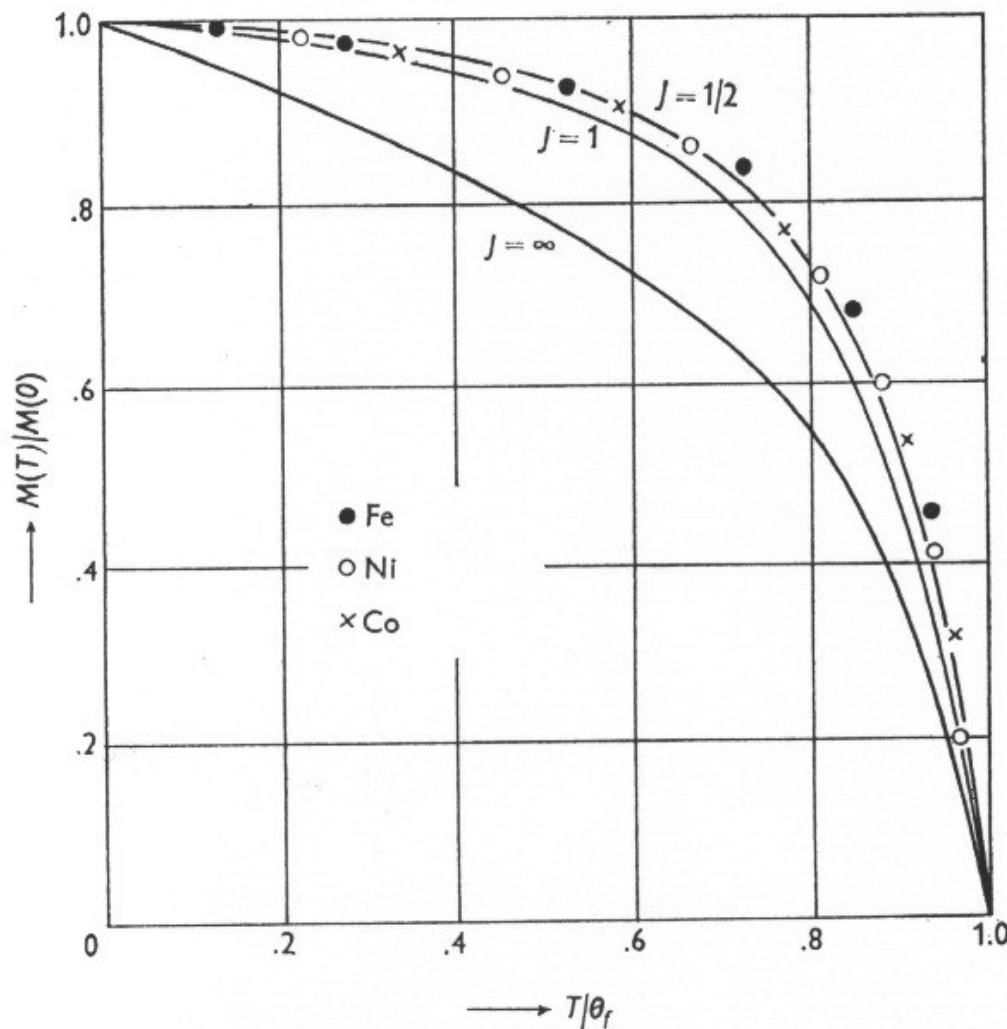
^aThe compositions of the alloys are given in weight percent unless otherwise stated.

^bThe maximum relative magnetic permeability $\mu_r(\text{max})$ is expressed here in units of $\mu_0 = 4\pi \times 10^{-7}$ N/A² and corresponds to the maximum value of B/H on the hysteresis loop in the first quadrant taken in increasing field.

Feromagnetické materiály – spontánní magnetizace



Feromagnetické materiály – spontánní magnetizace



Obr. 19.3. Spontánní magnetizace u Fe, Ni a Co jako funkce teploty. Křivky pro $J = \frac{1}{2}$, $J = 1$ a $J = \infty$ byly získány užitím rovnic (19.10) a (19.11).

Feromagnetické slitiny

Počet Bohrových magnetonů na atom

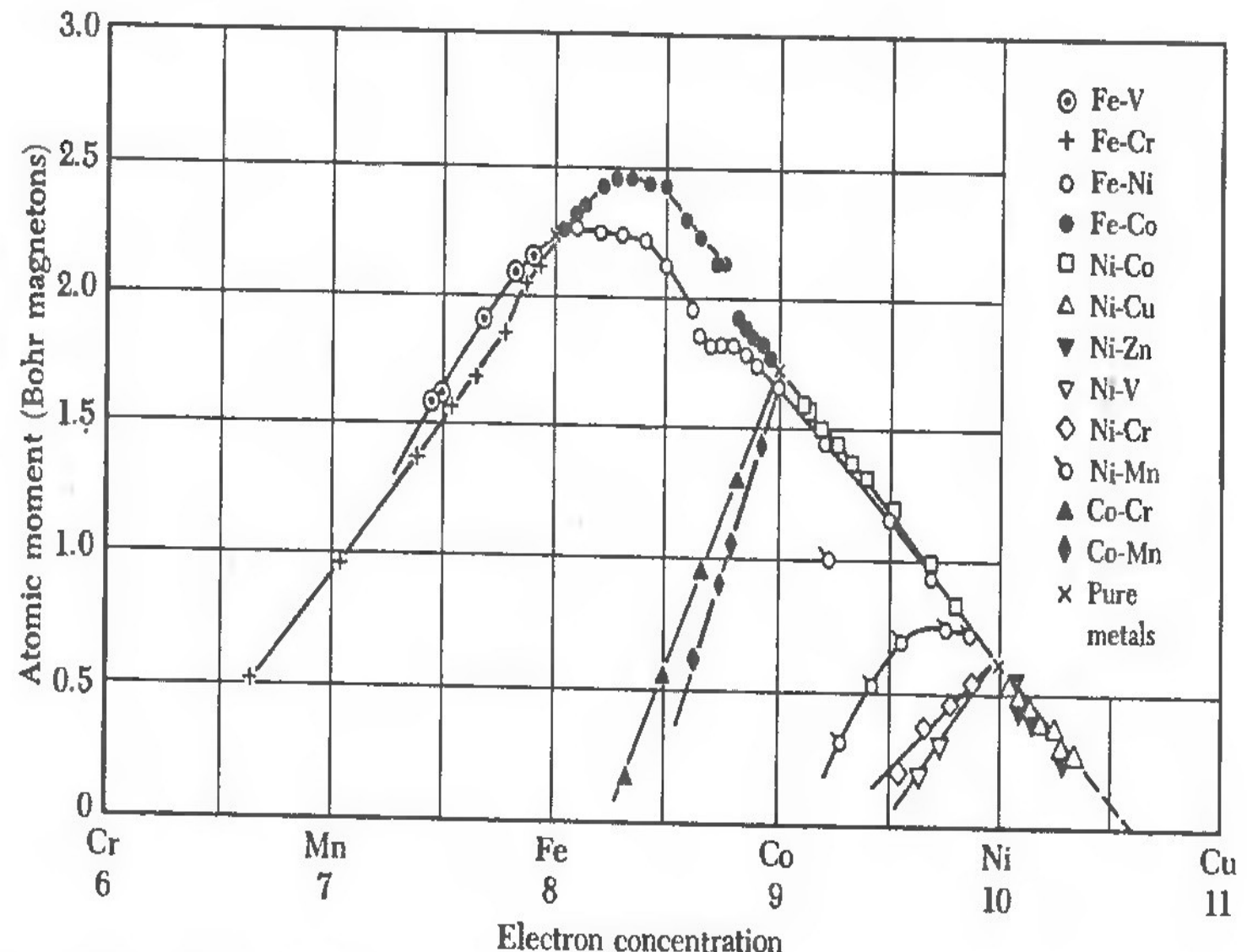


Figure 13 Average atomic moments of binary alloys of the elements in the iron group. (After Bozorth.)

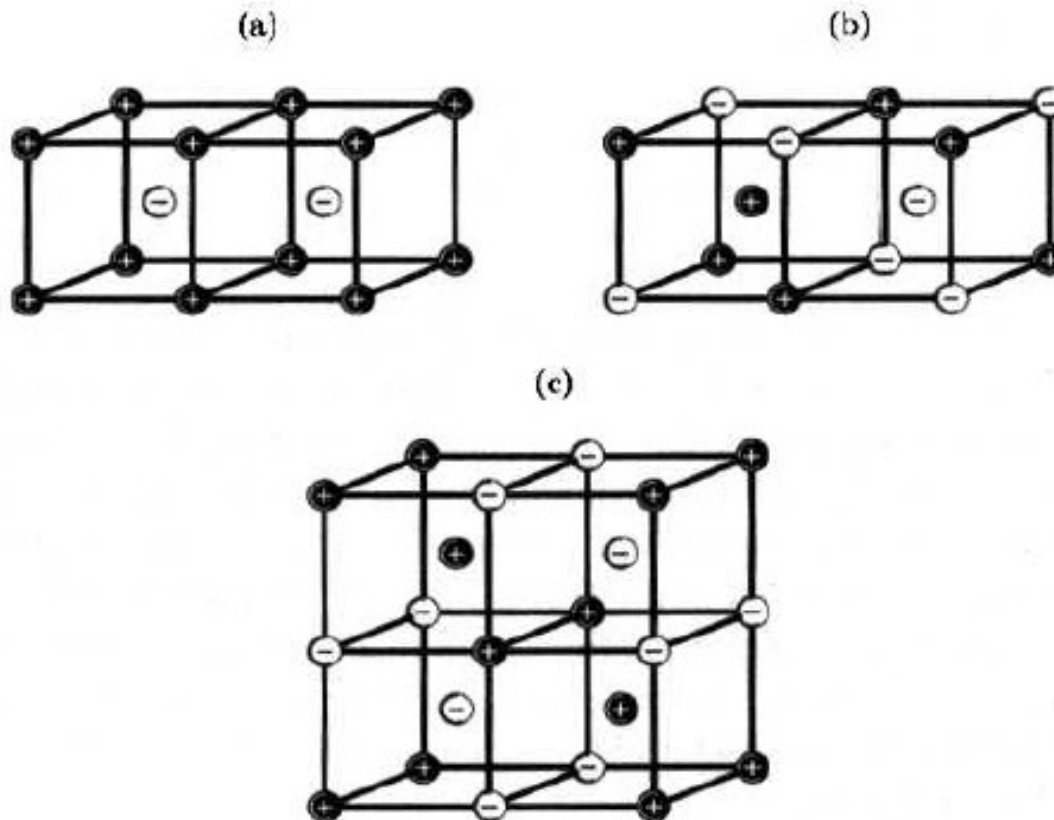
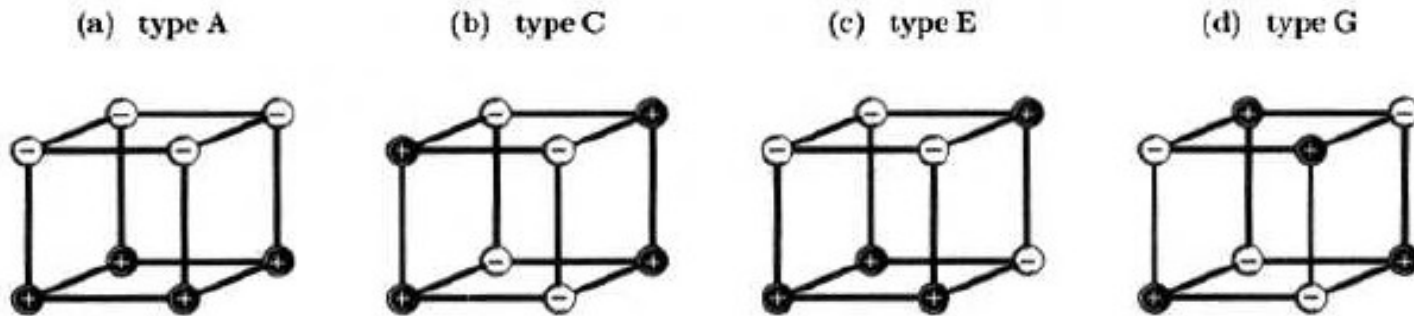
Antiferomagnetické látky

	T_N (K)	T_N (°C)	
Ce	12.5	-260.65	
Pr	25	-248	
Nd	19	-254	
Eu	90	-183	
Sm	14.8	-258.35	

Antiferomagnetické látky

	T_N (K)	θ (K)	J
MnF_2	67	-80	5/2
MnO	116	-510	5/2
CoO	292	-330	3/2
FeO	116	-610	2
Cr_2O_3	307	-485	3/2
$\alpha-Fe_2O_3$	950	-2000	5/2

Antiferromagnetické uspořádání v kubické prosté a bcc mřížce



Antiferomagnetické uspořádání – neutronová difrakce

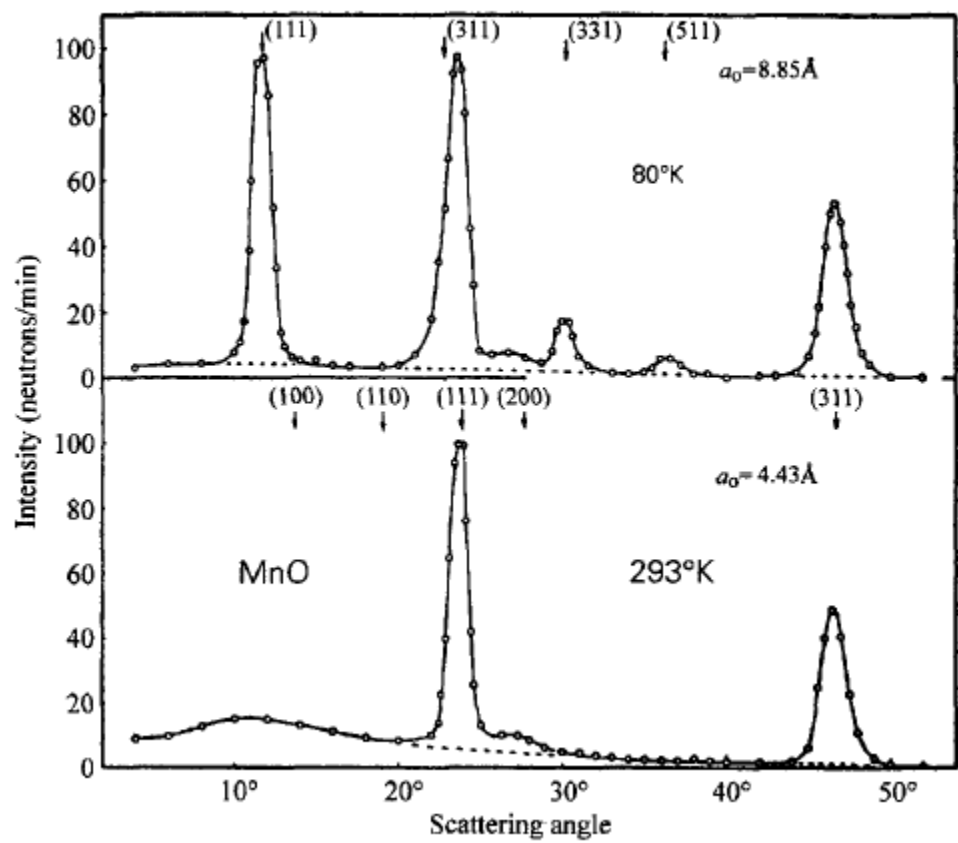
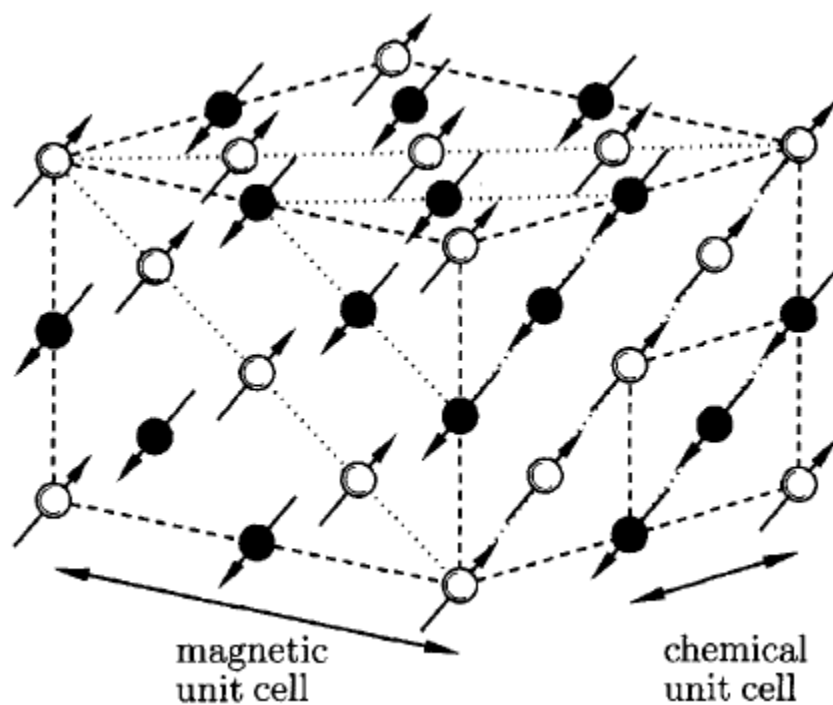
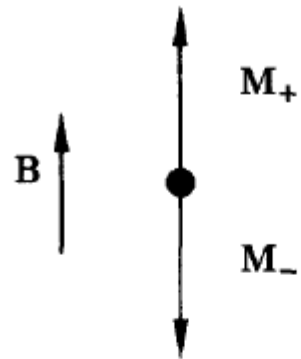


Fig. 5.19 Neutron diffraction patterns for MnO below and above T_N . After C. G. Shull, W. A. Strauser and E. O. Wollan, *Phys. Rev.*, **83**, 333 (1951).

Antiferomagnetické látky – typická závislost susceptibility na teplotě

(a)



(b)

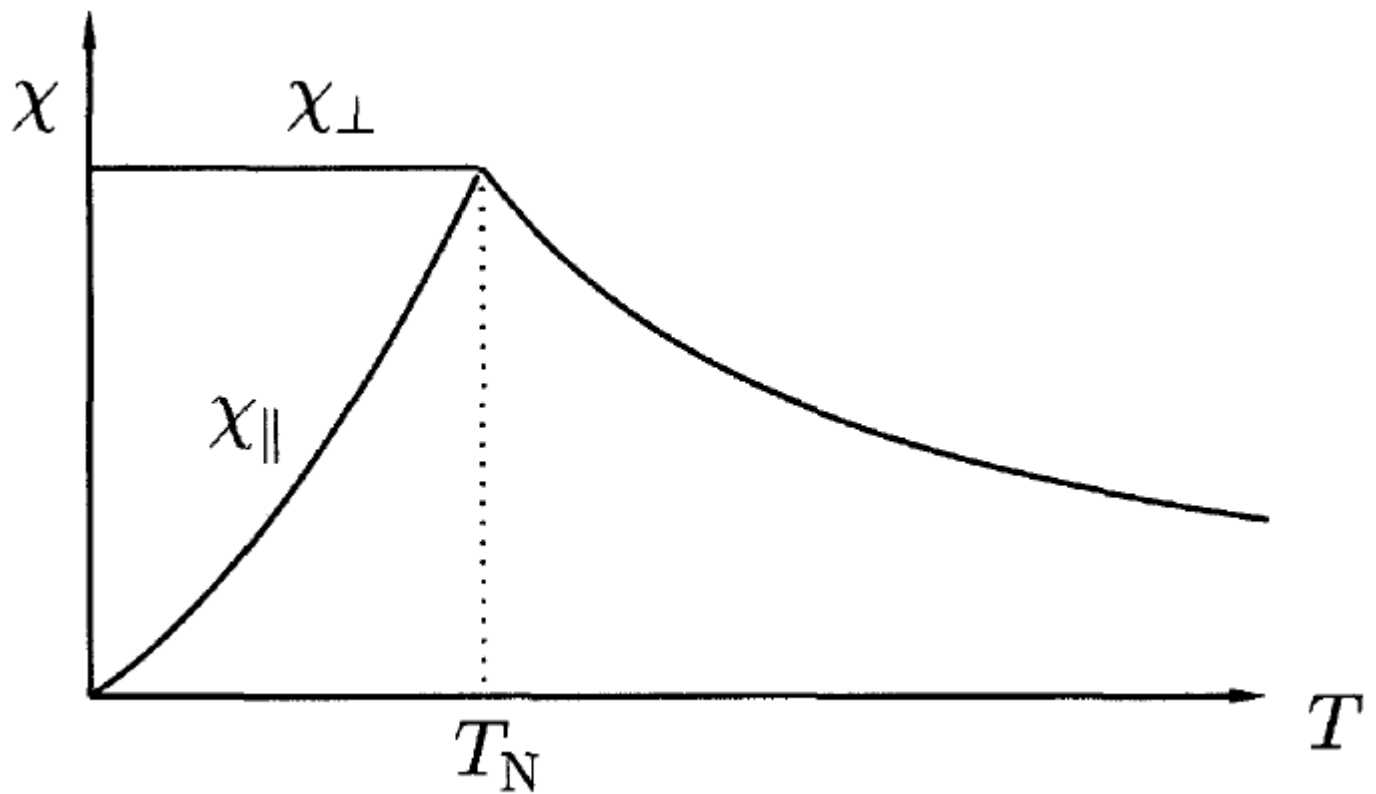
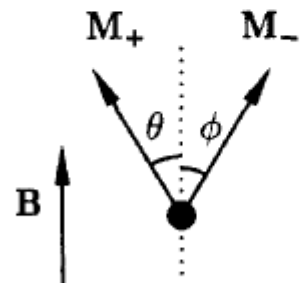


Fig. 5.10 A magnetic field is applied parallel to the sublattice magnetizations. (a) For small fields nothing happens and the system remains in the antiferromagnetic phase. (b) Above a critical field the system undergoes a spin-flop transition into a spin-flop phase.

Ferity

	T _c (°C)	N _{ef} /molekula	ρ (10 ⁶ Ω.cm)	M _s (T) při 0K
Fe ₃ O ₄	585	4.1		0.64
MgFe ₂ O ₄	440	1.1	1	
MnFe ₂ O ₄	300	4.6	0.02	0.70
CoFe ₂ O ₄	520	3.94	0.5	0.60
NiFe ₂ O ₄	585	2.3	2	0.38

	T _c (K)	N _{ef} /molekula	Kompenzační teplota (K)	M _s (T) při 0K
CuFe ₂ O ₄	728	1.3	-	0.20
Y ₃ Fe ₅ O ₁₂	560	5.0	-	0.25
Gd ₃ Fe ₅ O ₁₂	564	16.0	290	
Dy ₃ Fe ₅ O ₁₂	563	18.2	220	
Ho ₃ Fe ₅ O ₁₂	567	15.2	137	

Ferity

Spontánní
magnetizace feritů
 MeFe_2O_4 v závislosti
na teplotě

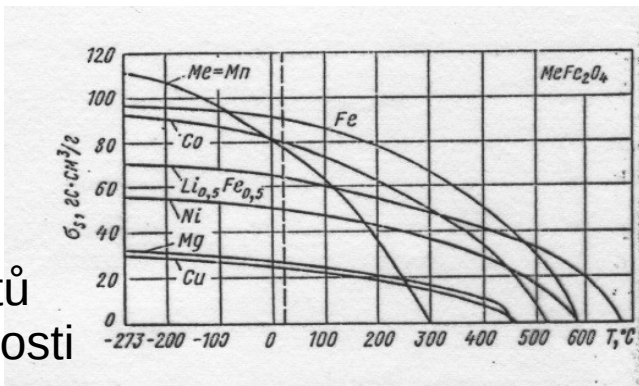


Рис. 29.2. Зависимость удельной намагниченности насыщения σ_s для некоторых простых ферритов-шпинелей от температуры [5]

Směsi feritů s
 ZnFe_2O_4
Počet
Bohrových
magnetonů na
molekulu

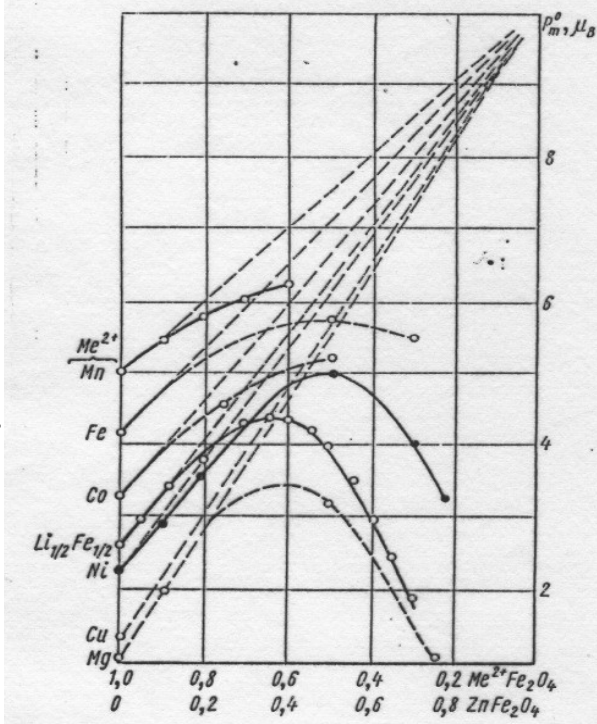


Рис. 29.3. Магнитные моменты насыщения p_m^0 при 0°К некоторых смешанных ферритов, полученных замещением магнитных ионов двухвалентного металла Me^{2+} немагнитными ионами цинка (Me^{2+} — один из ионов Mn , Fe , Co , Ni , Cu или Li , Fe) [37]

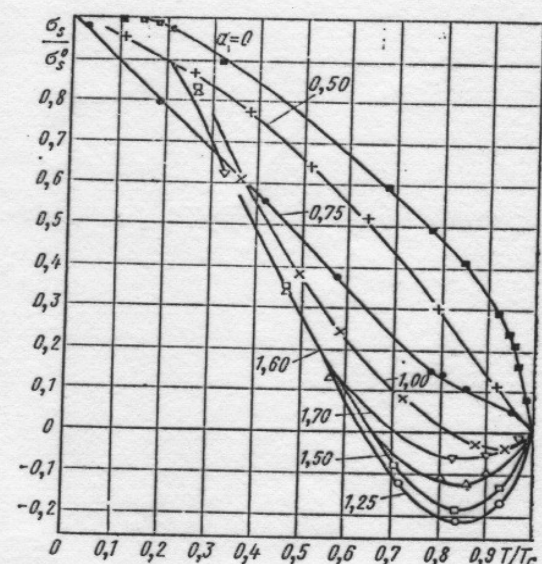


Рис. 29.4. Зависимость относительной намагниченности насыщения σ_s/σ_s^0 от приведенной температуры T/T_C для литиевых ферритов-хромитов $\text{Li}_{0,5}\text{Fe}_{2,5-x}\text{Cr}_x\text{O}_4$ [68]

Spontánní
magnetizace feritu
 $\text{Li}_{0,5}\text{Fe}_{2,5-x}\text{Cr}_x\text{O}_4$

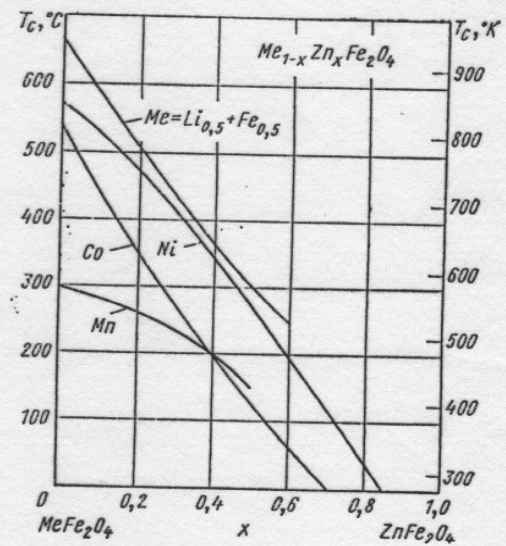
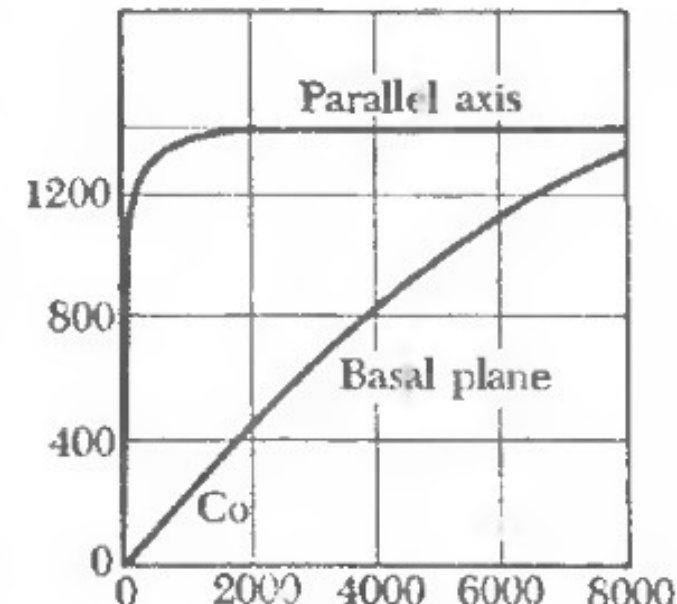
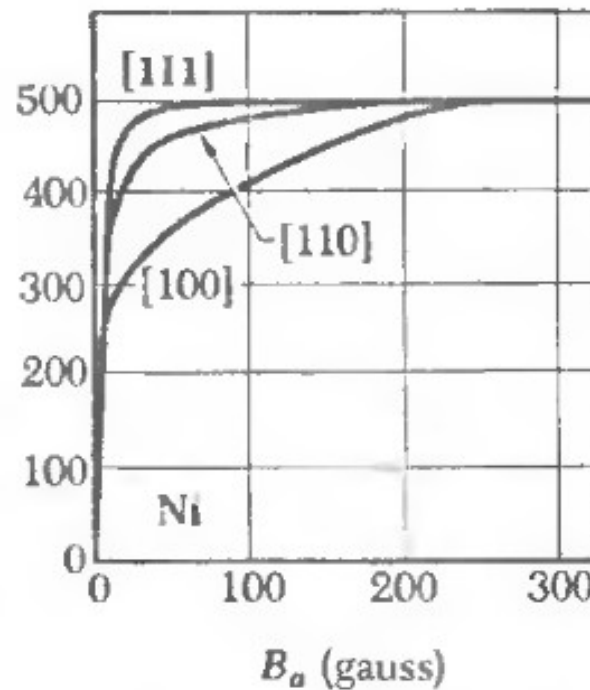
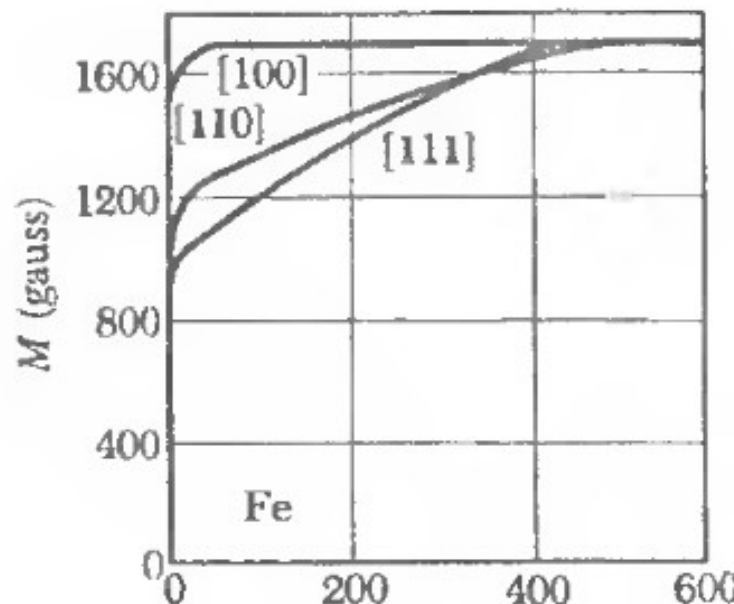


Рис. 29.5. Зависимость точки Кюри T_C некоторых смешанных ферритов типа $\text{Me}_{1-x}\text{Zn}_x\text{Fe}_2\text{O}_4$ от концентрации цинка [5]

Směsi feritů s
 ZnFe_2O_4
Curieova
teplota

Krystalová anizotropie ve feromagnetických materiálech



Směr snadné magnetizace:

[100]

[111]

[001]

Směr obtížné magnetizace:

[111]

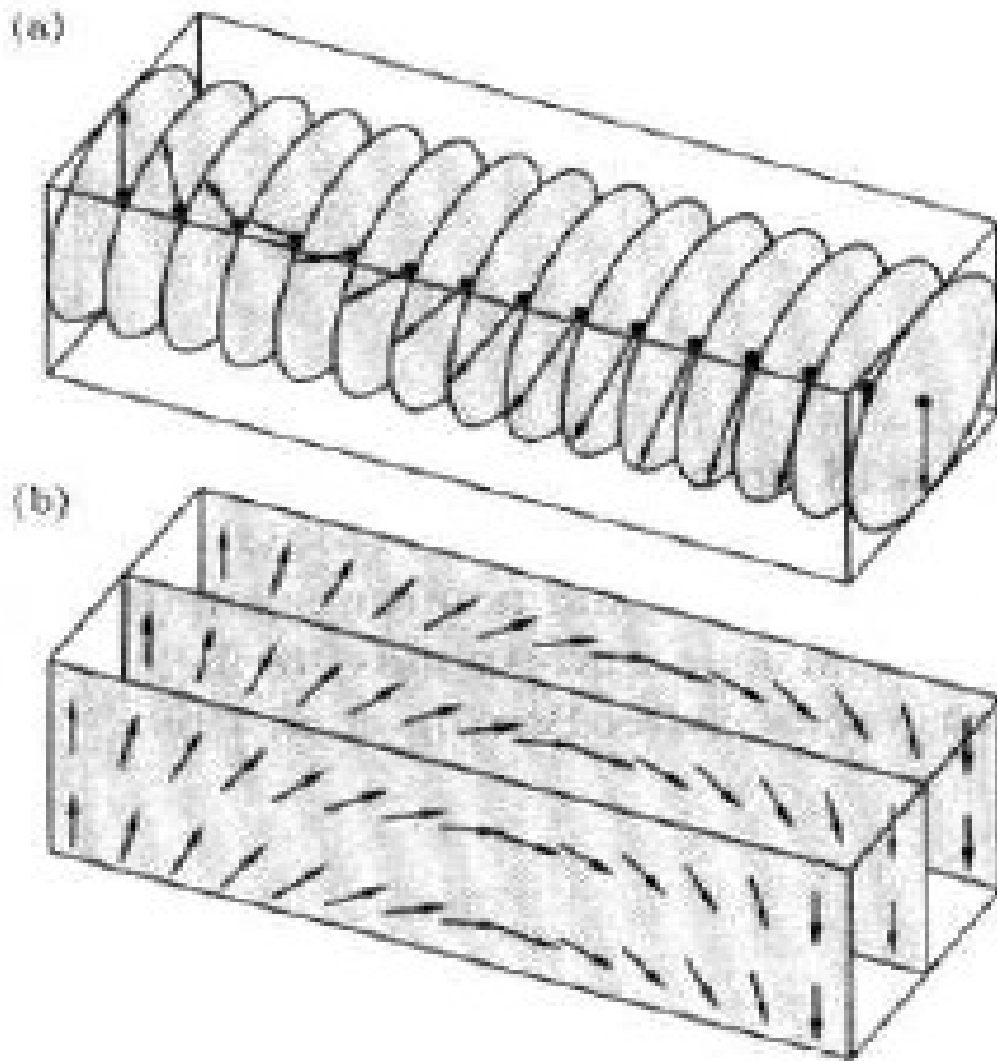
[100]

v rovině kolmé

Kittel:

Blundell, Magnetism in solid state, Oxford university press, 2002 uvádí chybně

Doménové stěny ve feromagnetech



Rozměr stěny železo
cca 40nm
Jiles (1998)

Fig. 6.20 (a) A Bloch wall. (b) A Néel wall.

Kritické exponenty ve feromagnetech

Table 1 Critical point exponents for ferromagnets

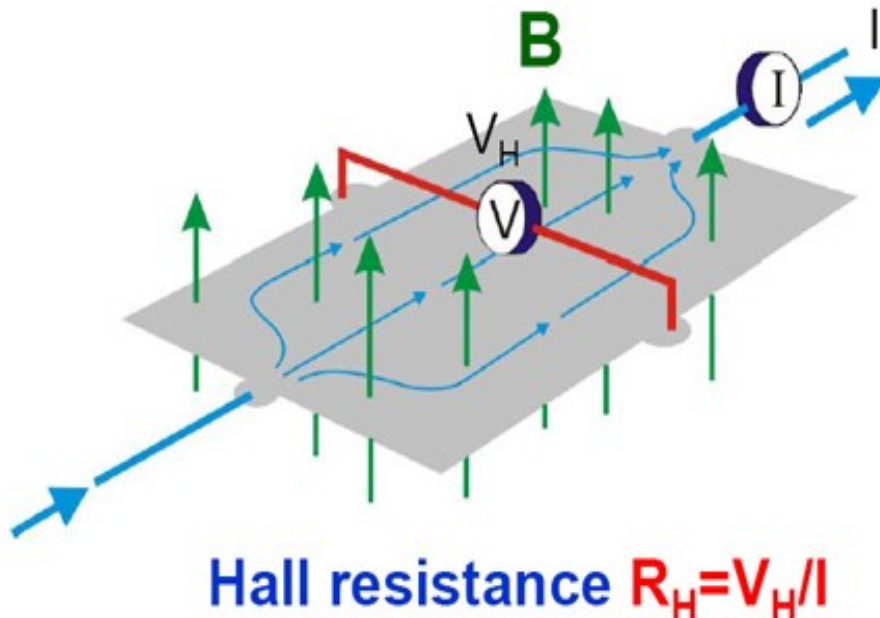
As $T \rightarrow T_c$ from above, the susceptibility χ becomes proportional to $(T - T_c)^{-\gamma}$; as $T \rightarrow T_c$ from below, the magnetization M_s becomes proportional to $(T_c - T)^\beta$. In the mean field approximation, $\gamma = 1$ and $\beta = \frac{1}{2}$.

	γ	β	T_c , in K
Fe	1.33 ± 0.015	0.34 ± 0.04	1043
Co	1.21 ± 0.04	—	1388
Ni	1.35 ± 0.02	0.42 ± 0.07	627.2
Gd	1.3 ± 0.1	—	292.5
CrO ₂	1.63 ± 0.02	—	386.5
CrBr ₃	1.215 ± 0.02	0.368 ± 0.005	32.56
EuS	—	0.33 ± 0.015	16.50

Experimental data collected by H. E. Stanley.

Hall Effect

Edwin H. Hall (1879)



$$R_H = B/dnq$$

Magnetické pole

Tloušťka

Koncentrace nositelů náboje

Obří magnetorezistence Giant magnetoresistance

NC 2007

Albert Fert

Peter Gruenberg

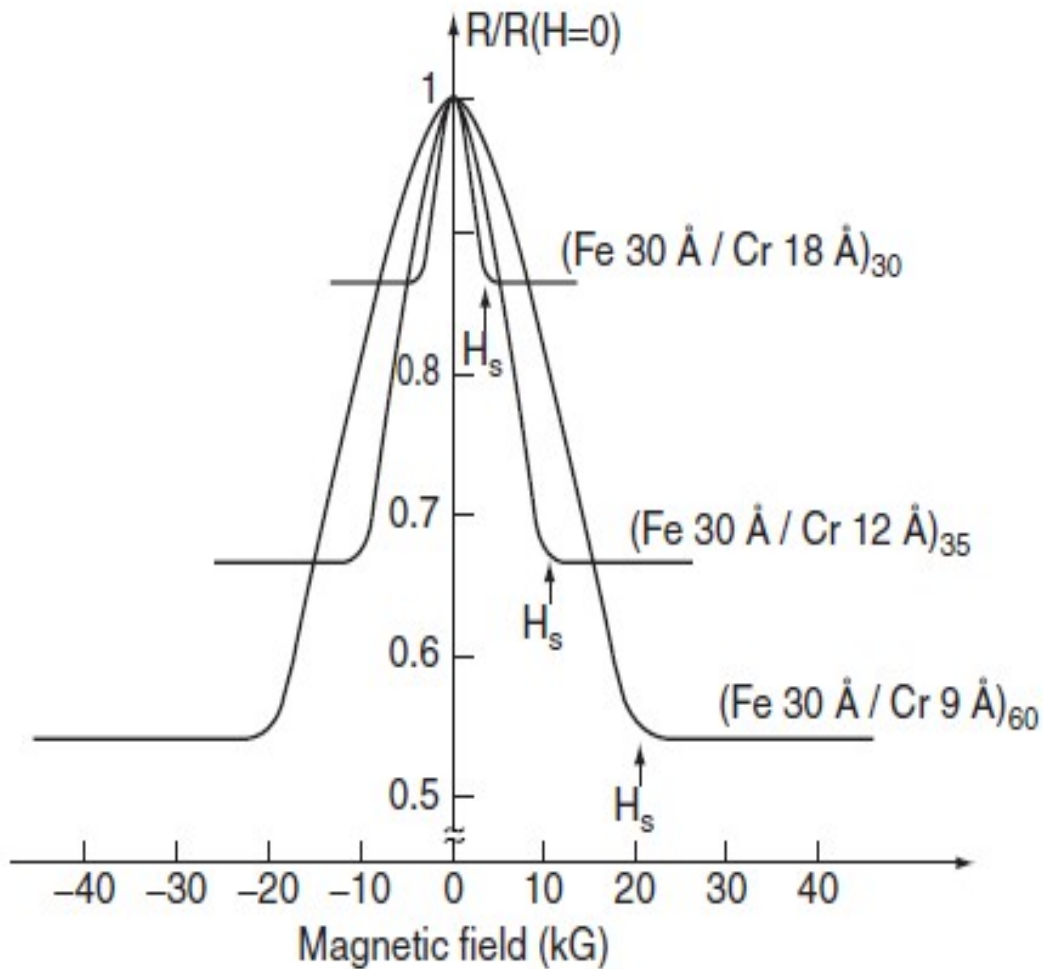


Figure W17.2. Experimental observations of giant longitudinal magnetoresistance $R(H)/R(0)$ in three different (001)Fe/(001)Cr magnetic multilayers at $T = 4.2$ K. [From M. N. Baibich et al., *Phys. Rev. Lett.*, **61**, 2472 (1988). Copyright 1988 by the American Physical Society.]

Bez pole vrstvy uspořádány antiferomagneticky

Gersten, Smith, The physics and chemistry of materials, Wiley 2001.

Obří magnetorezistence Giant magnetoresistace

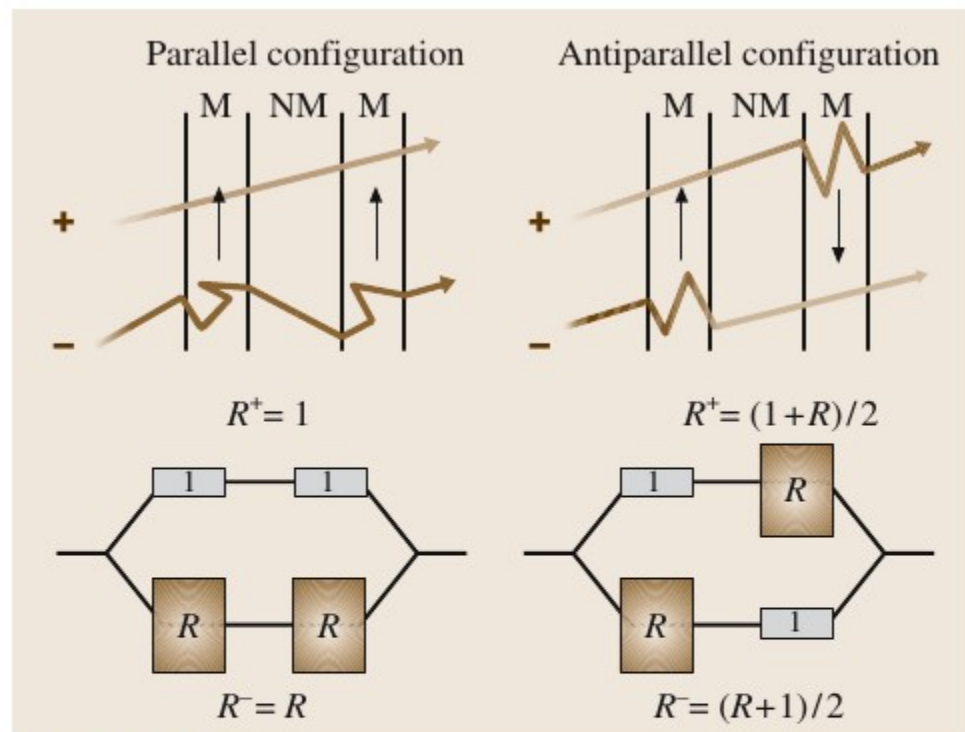


Fig. 5.3-21 Schematic picture of the GMR mechanism. The electron trajectories between two scatterings are represented by *straight lines* and the scatterings by abrupt changes in the direction. The *signs* + and – are for spins $S_z = 1/2$ and $S_z = -1/2$, respectively. The *arrows* represent the majority-spin direction in the magnetic layers. M = magnetic, NM = nonmagnetic. (After [3.95])

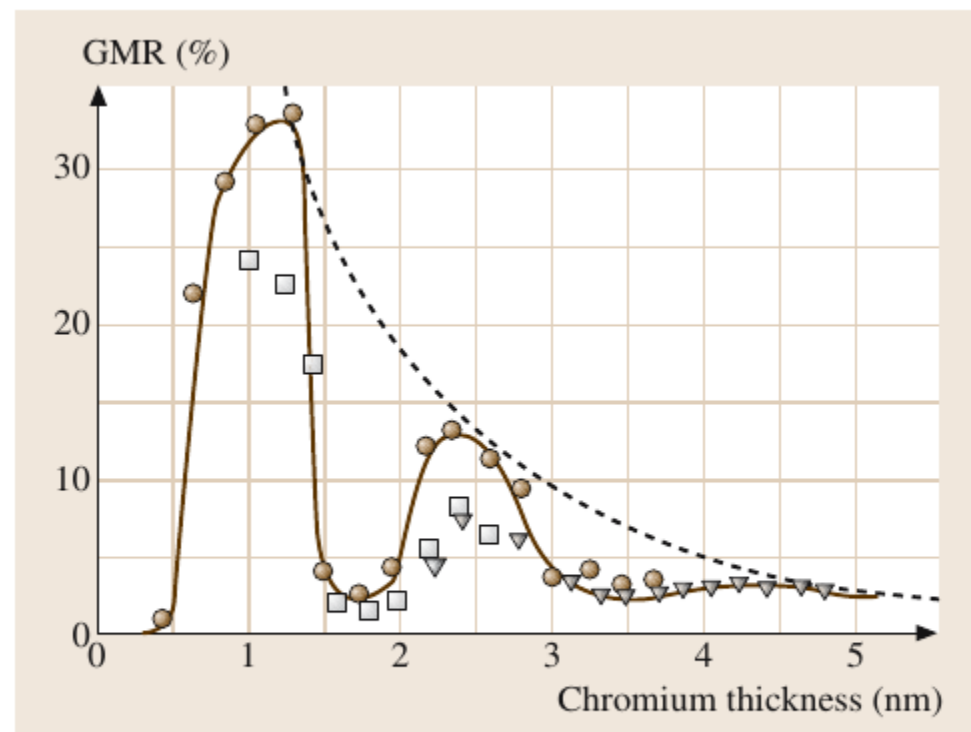


Fig. 5.3-20 Dependence of the GMR ratio of an Fe/Cr multilayer on Cr thickness. (After [3.94])

Kolosální magnetorezistence

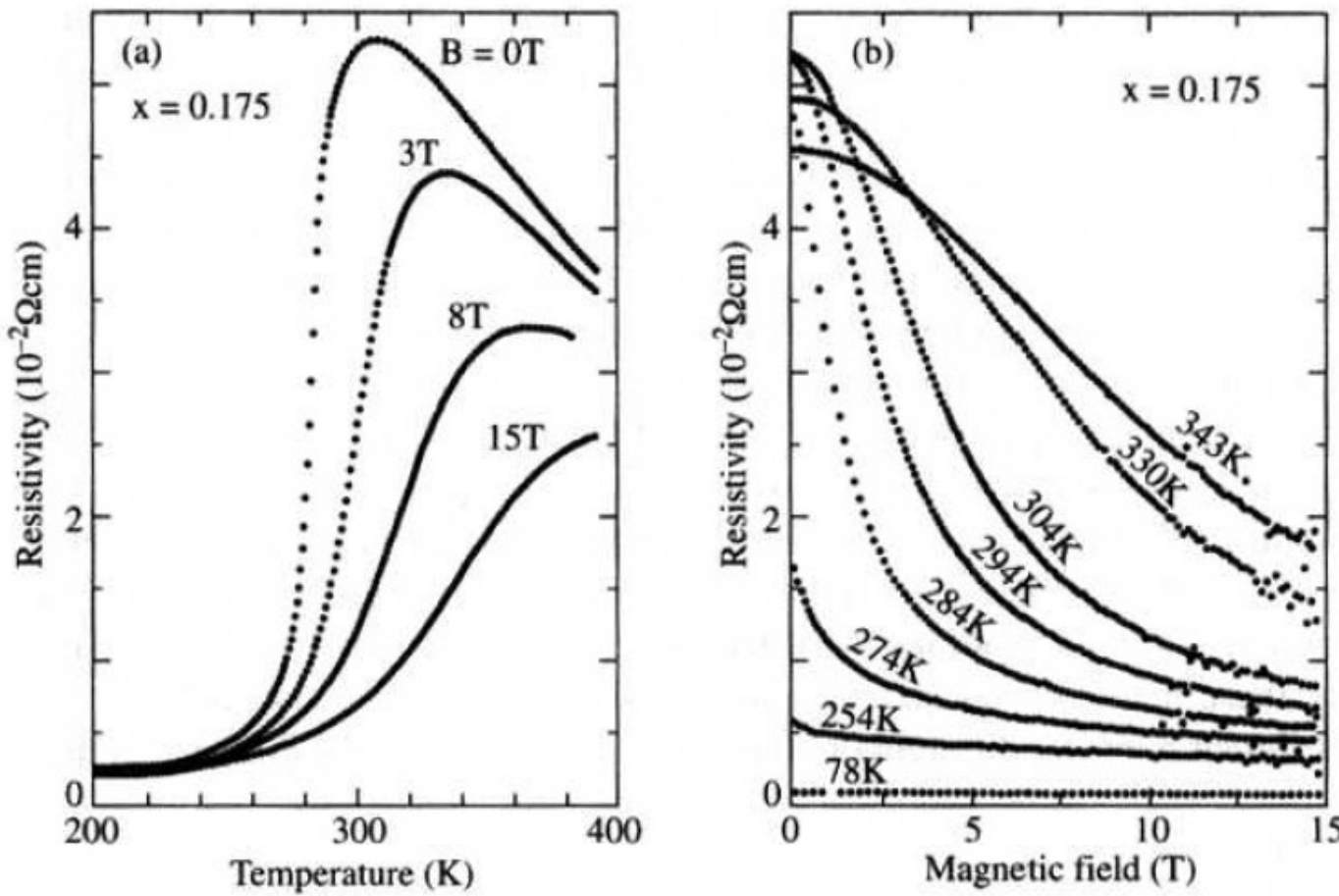


Fig. 8.23 Colossal magnetoresistance in $\text{La}_{1-x}\text{Sr}_x\text{MnO}_3$ for $x = 0.175$. (a) Temperature dependence of the resistivity. (b) Isothermal magnetoresistance. After Tokura *et al.* 1994.

Kondův jev

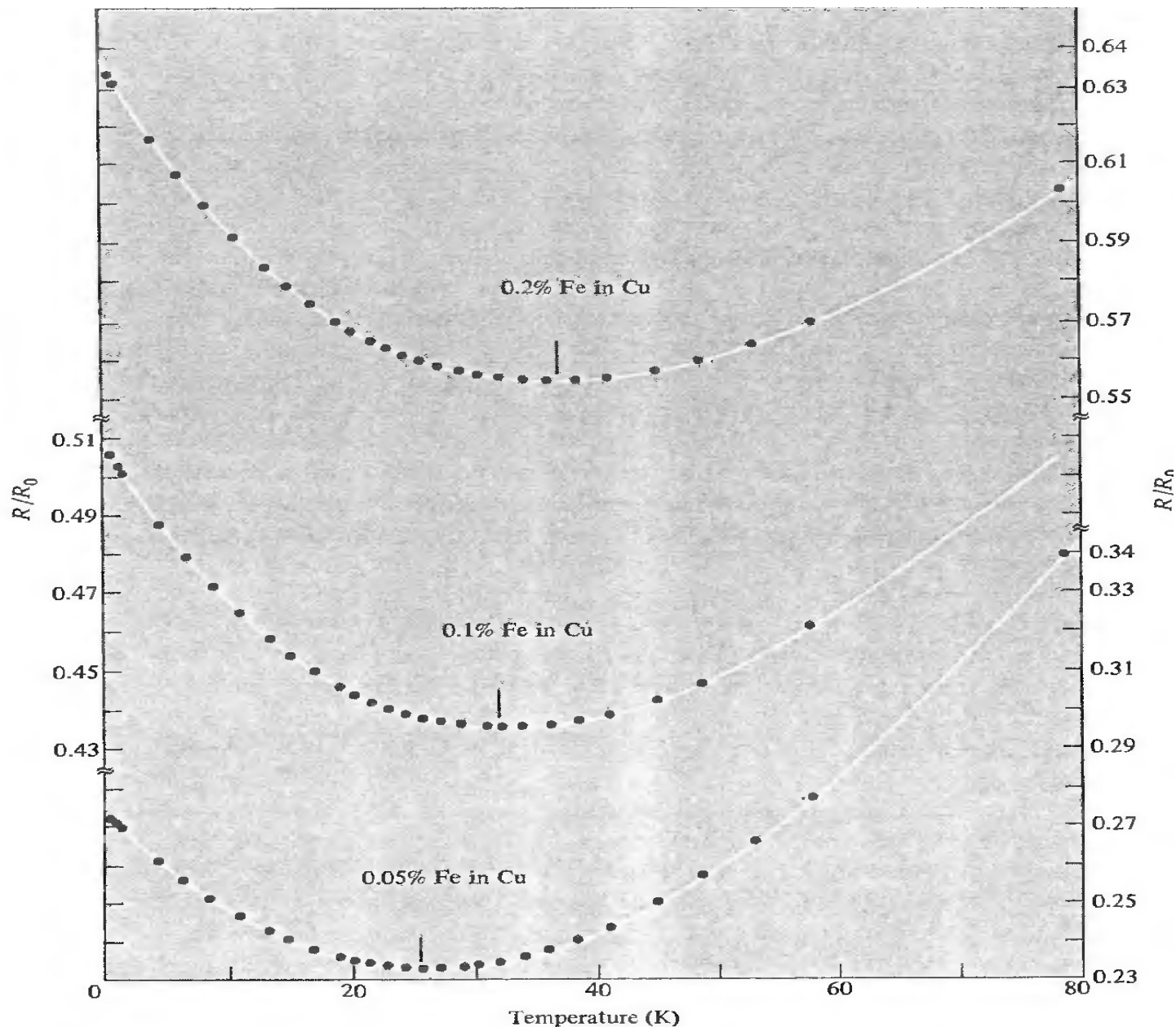
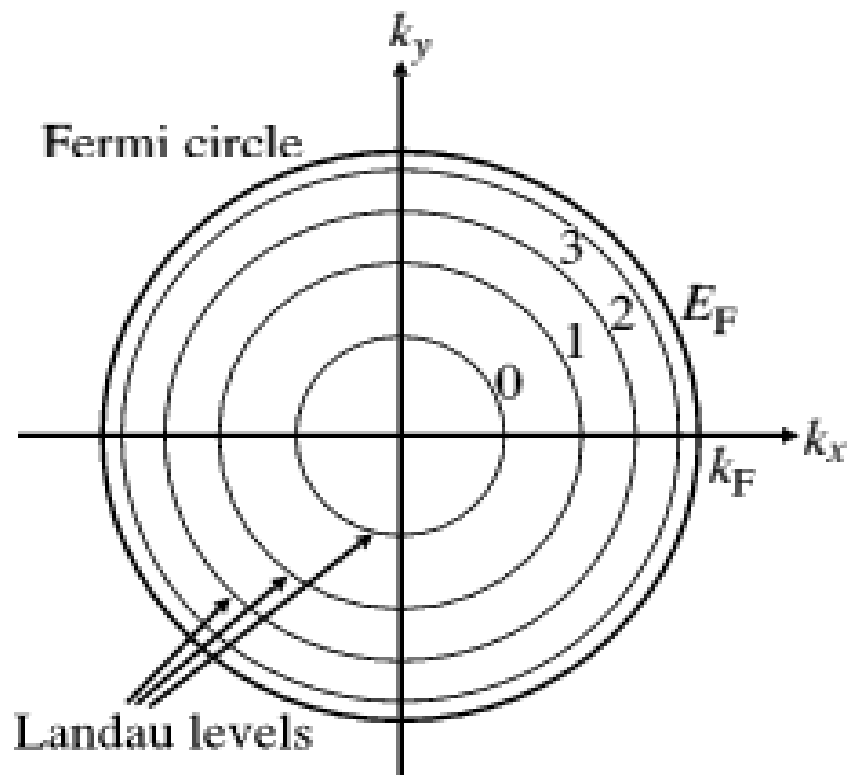


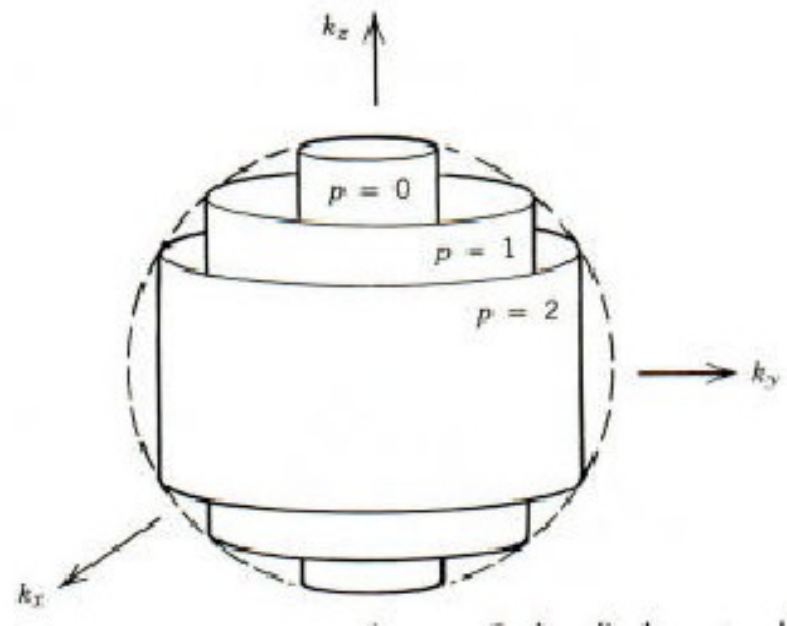
Figure 32.3

The resistance minimum for various dilute alloys of iron in copper. (R_0 is the resistivity at 0°C.)

Landaovy hladiny



$$E_{n,k_z} = \left(n + \frac{1}{2} \right) \hbar \omega_c + \frac{\hbar^2 k_z^2}{2m^*}$$

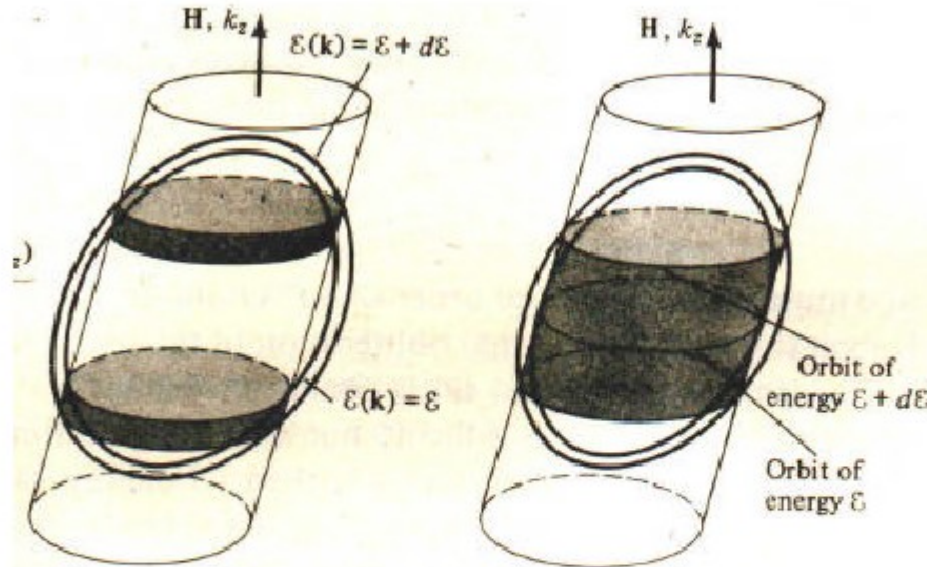


Landaovy hladiny

Oscillation of the DOS at the Fermi energy

w/o extremal orbit

w/ extremal orbit



- The number of states at E_F are highly enhanced when there are extremal orbits on the FS
- There are extremal orbits at regular interval of $1/B$

$$P(B^{-1}) = \frac{2\pi e}{\hbar S}$$

S - extremální řez Fermiho plochy
P - perioda oscilací v $1/B$

De Haas–van Alphen effect

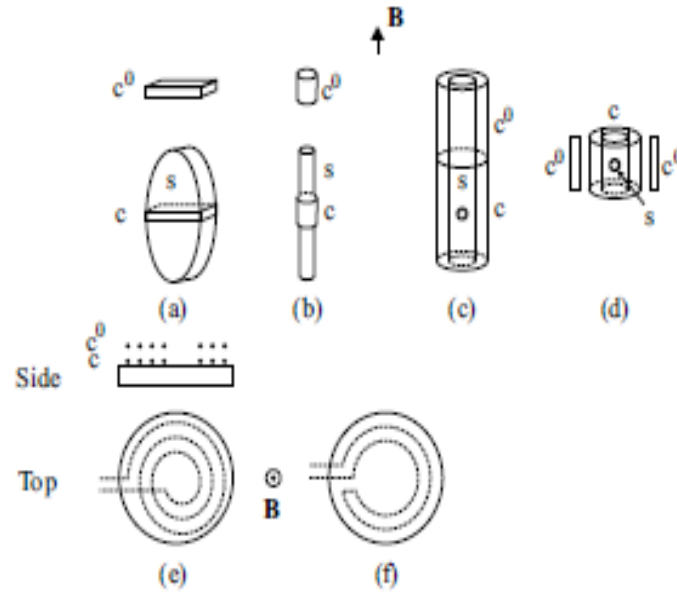


Figure 9.8: Coils for the observation of the de Haas–van Alphen effect. For each set, c is the coil flux-linked to the sample and c^0 is the compensating coil, only weakly flux-linked to the sample: (a) c is wound around the centre of a disc-like sample; (b) c is wound around a sample cut into a cylinder; (c) a small sample inside colinear coils c and c^0 ; (d) small sample inside coaxial coils c and c^0 ; (e) side and top views of a coil evaporated down onto a thin sample; (f) as (e) but with only a single annular turn. In both (e) and (f) c^0 has not been shown. (Based on figures in *Magnetic oscillations in metals*, by David Shoenberg (Cambridge University Press, Cambridge 1984).)

$$V = \alpha \frac{dM}{dB} \frac{dB}{dt}.$$

De Haas-van Alphen jev

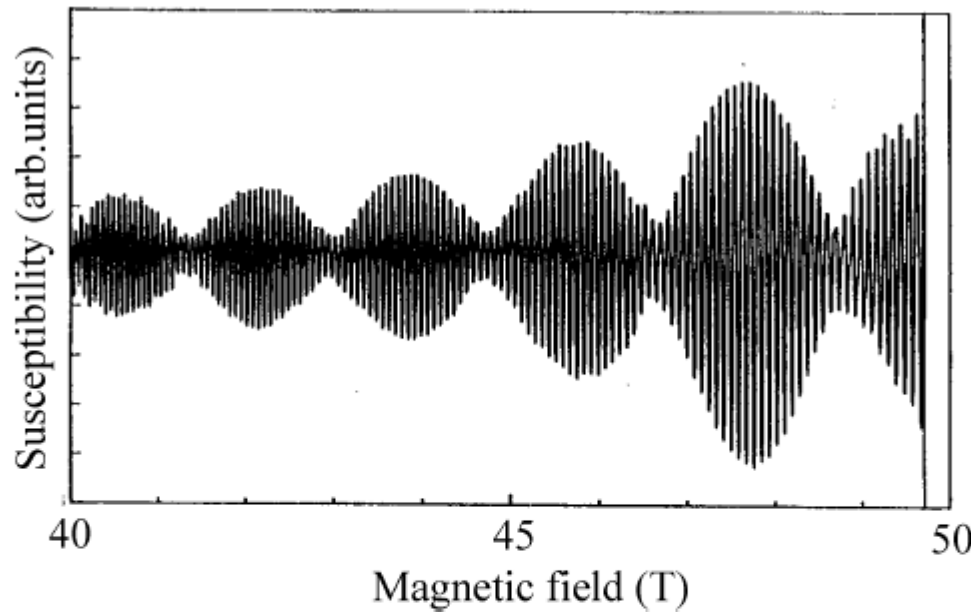


Figure 9.9: de Haas-van Alphen oscillations in Pt at 4.2 K with B parallel to [111]. The data have been recorded using a pulsed magnetic field. Note the presence of two frequencies of oscillations due to two extremal orbits about the Fermi surface. The y axis, labelled “susceptibility”, represents the voltage V induced in the coil divided by (dB/dt) , leaving a quantity proportional to the differential susceptibility (dM/dB) (see Equation 9.34). (Data from S. Askenazy, Physica B 201, 26 (1994).)

De Haas-van Alphen effect – dog's bone orbit

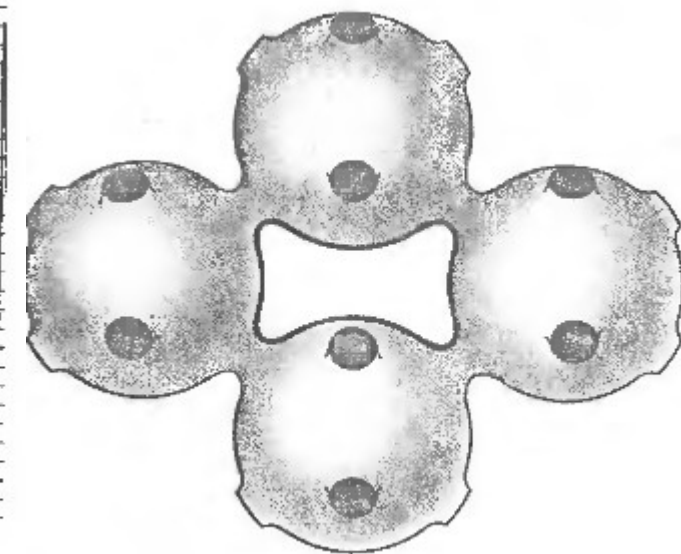
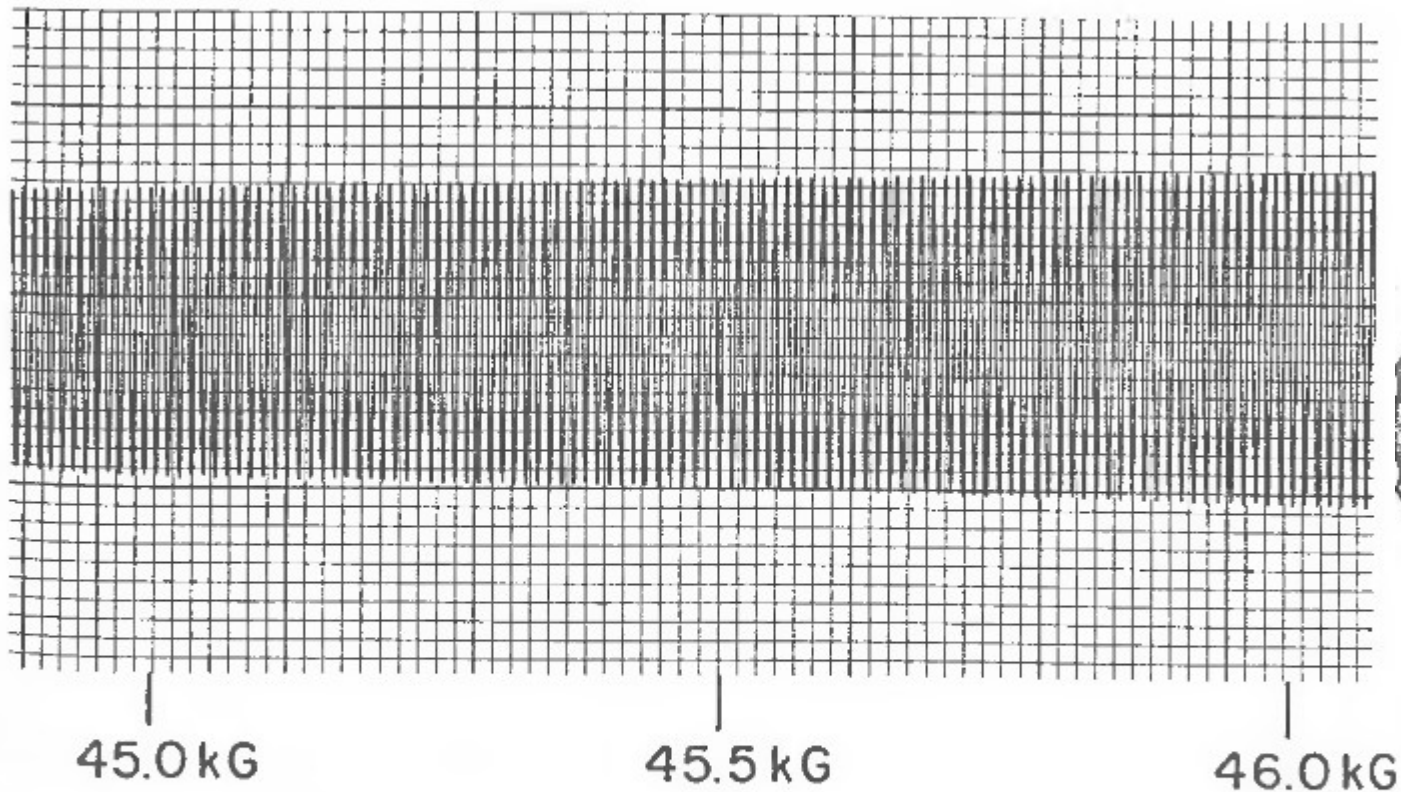


Figure 31 De Haas-van Alphen effect in gold with $\mathbf{B} \parallel [110]$. The oscillation is from the dog's bone orbit of Fig. 30. The signal is related to the second derivative of the magnetic moment with respect to field. The results were obtained by a field modulation technique in a high-homogeneity superconducting solenoid at about 1.2 K. (Courtesy of I. M. Templeton.)

De Haas-van Alphen effect

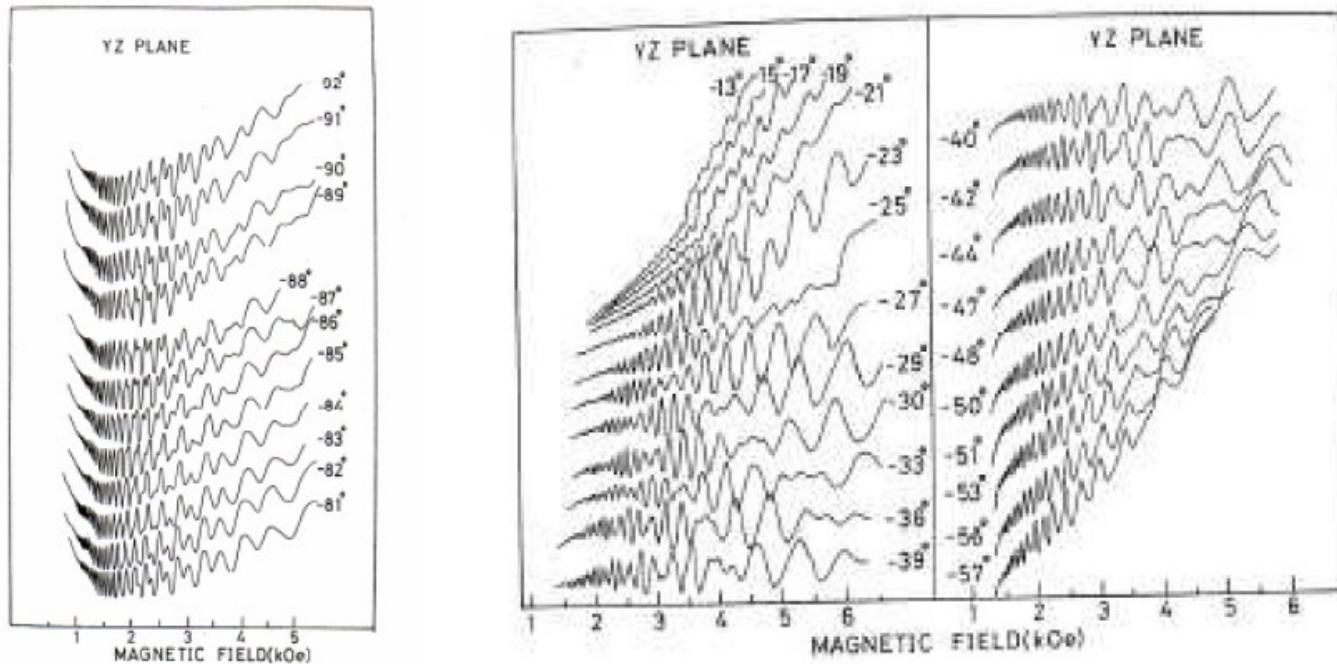
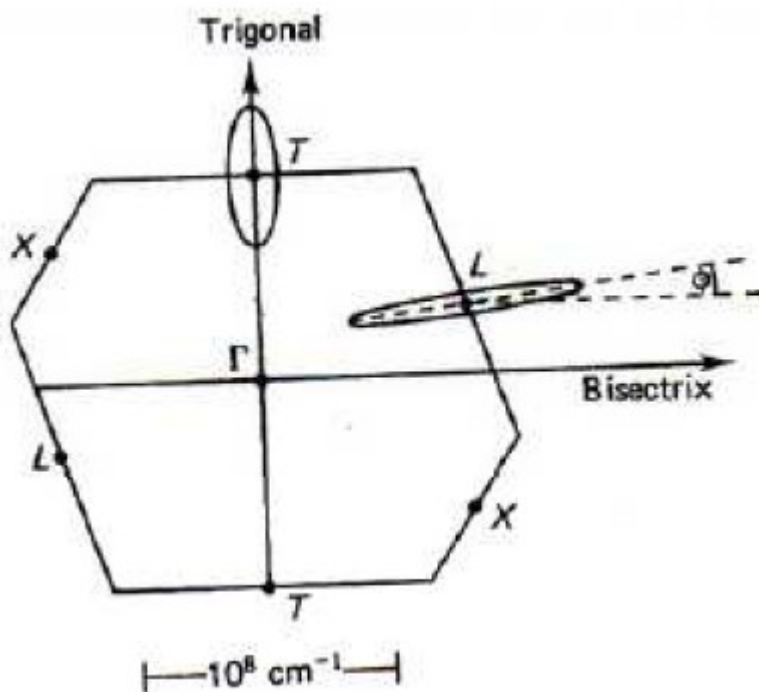
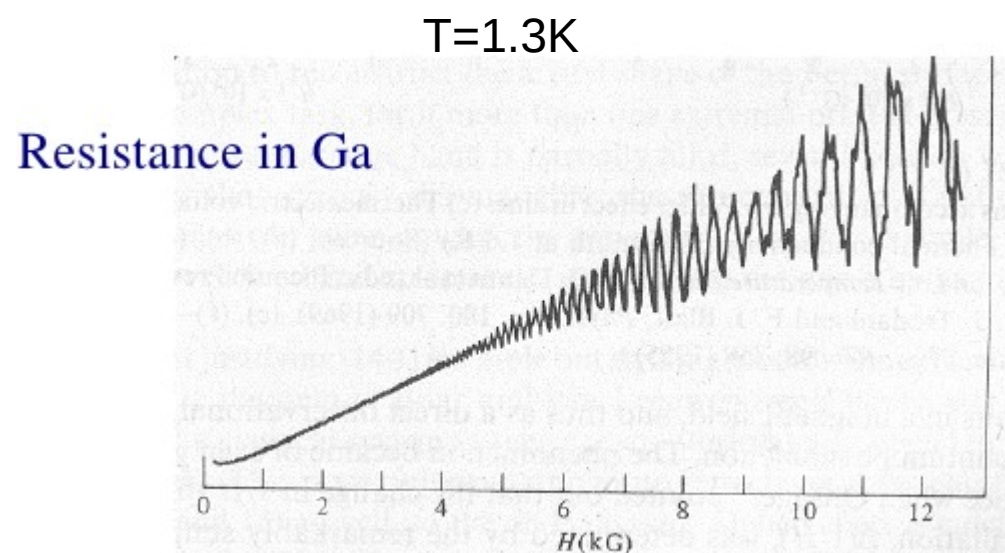
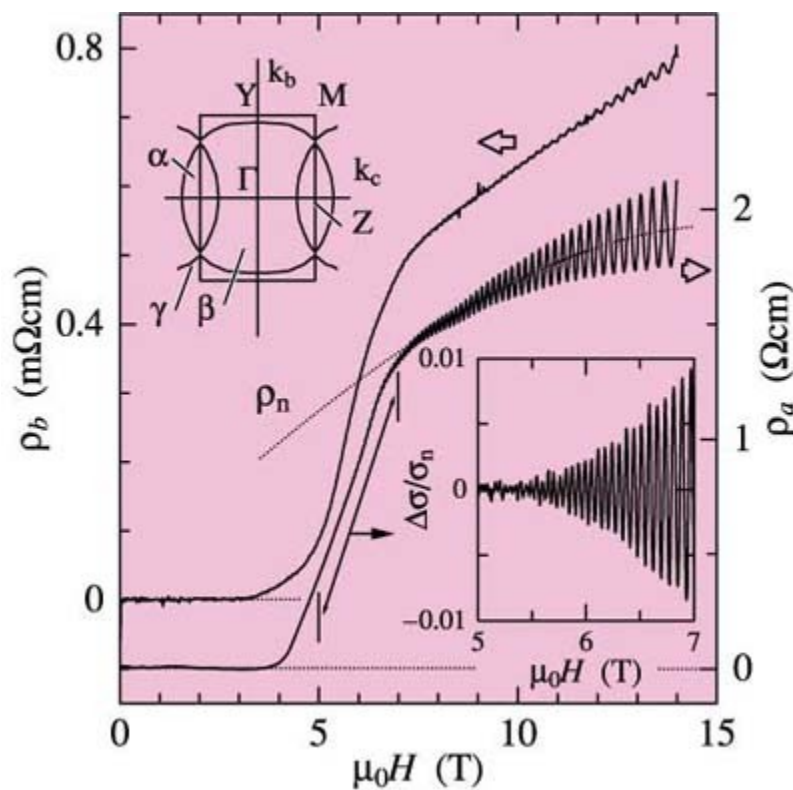


Fig. 7 The dHvA effect of Bi in the YZ plane. $T = 1.5$ K. This signal corresponds to the first harmonics ($\partial M / \partial h$).



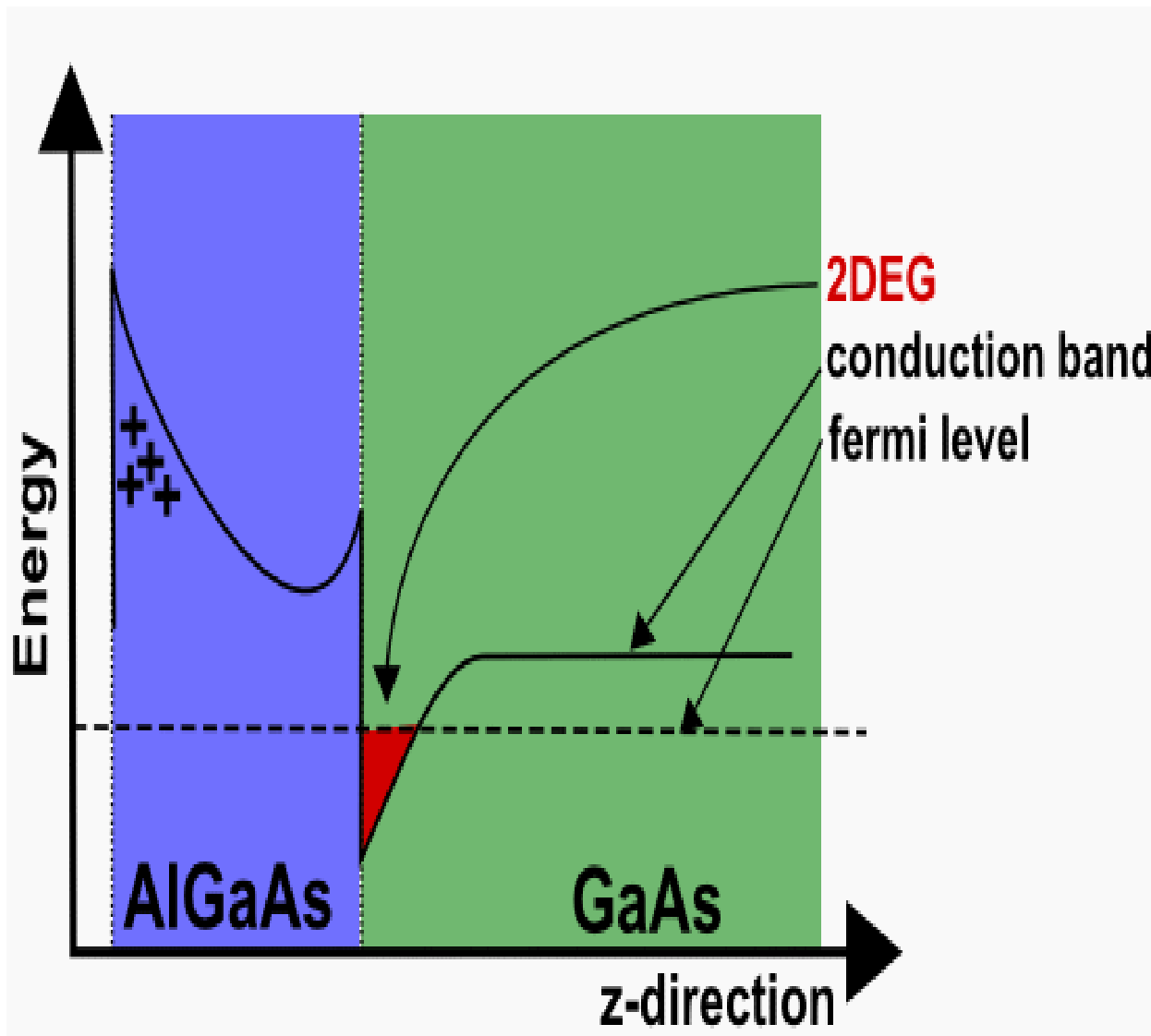
Shubnikovův – de Haasův jev



Shubnikov - de Haas (SdH) oscillations are observed in the superconducting state of the quasi two dimensional organic superconductor κ -(BEDT-TTF)₂Cu(NCS)₂. The SdH oscillations can be observed on the broad resistive transition curve down to about 5 T at 0.5 K, where the resistivity becomes about 30 % of the normal state value. The additional damping of the SdH oscillation amplitude in the superconducting state in comparison with the normal state damping described by the Lifshitz - Kosevich formula is found below about 7 T as well as that of the de Haas - van Alphen oscillations. A novel strong damping effect is found in only the SdH effect in the quantum vortex slush region strongly affected by quantum fluctuations.

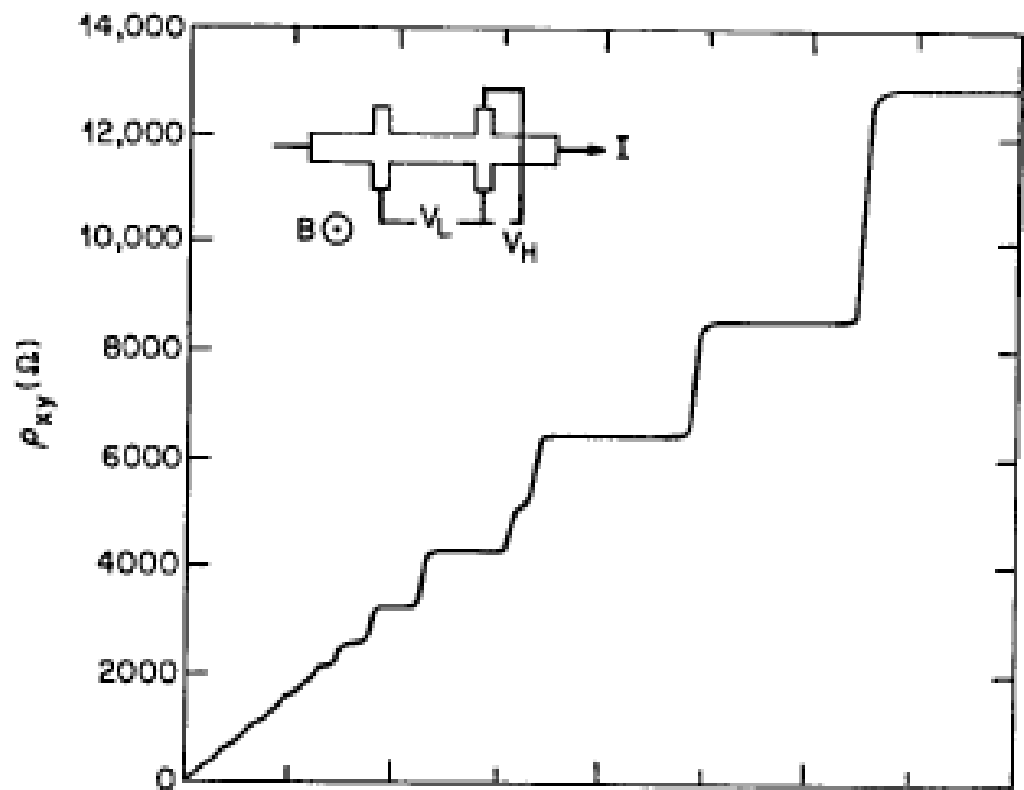
Kvantový Hallův jev

2D elektronový plyn – povrch polovodiče



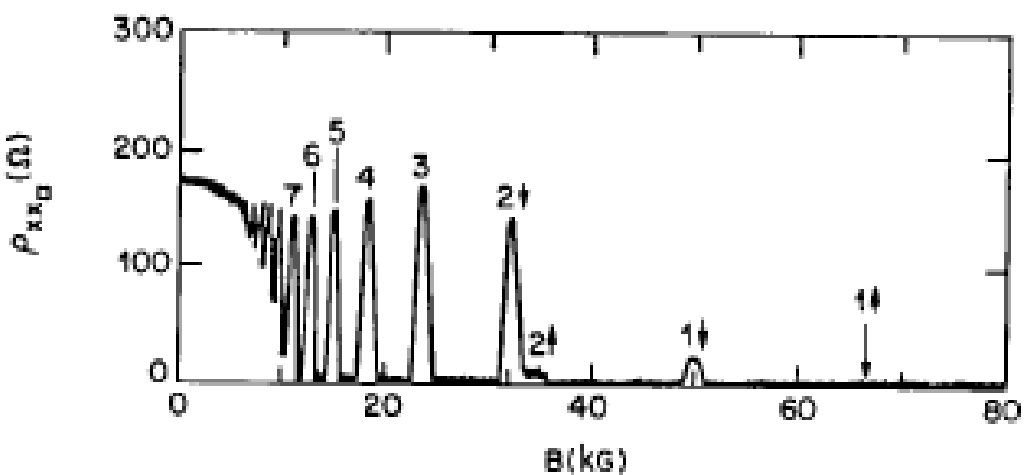
Kvantový Hallův jev – 2D elektronový systém

Kvantované Hallovo napětí – nezávislé na kvalitě materiálu



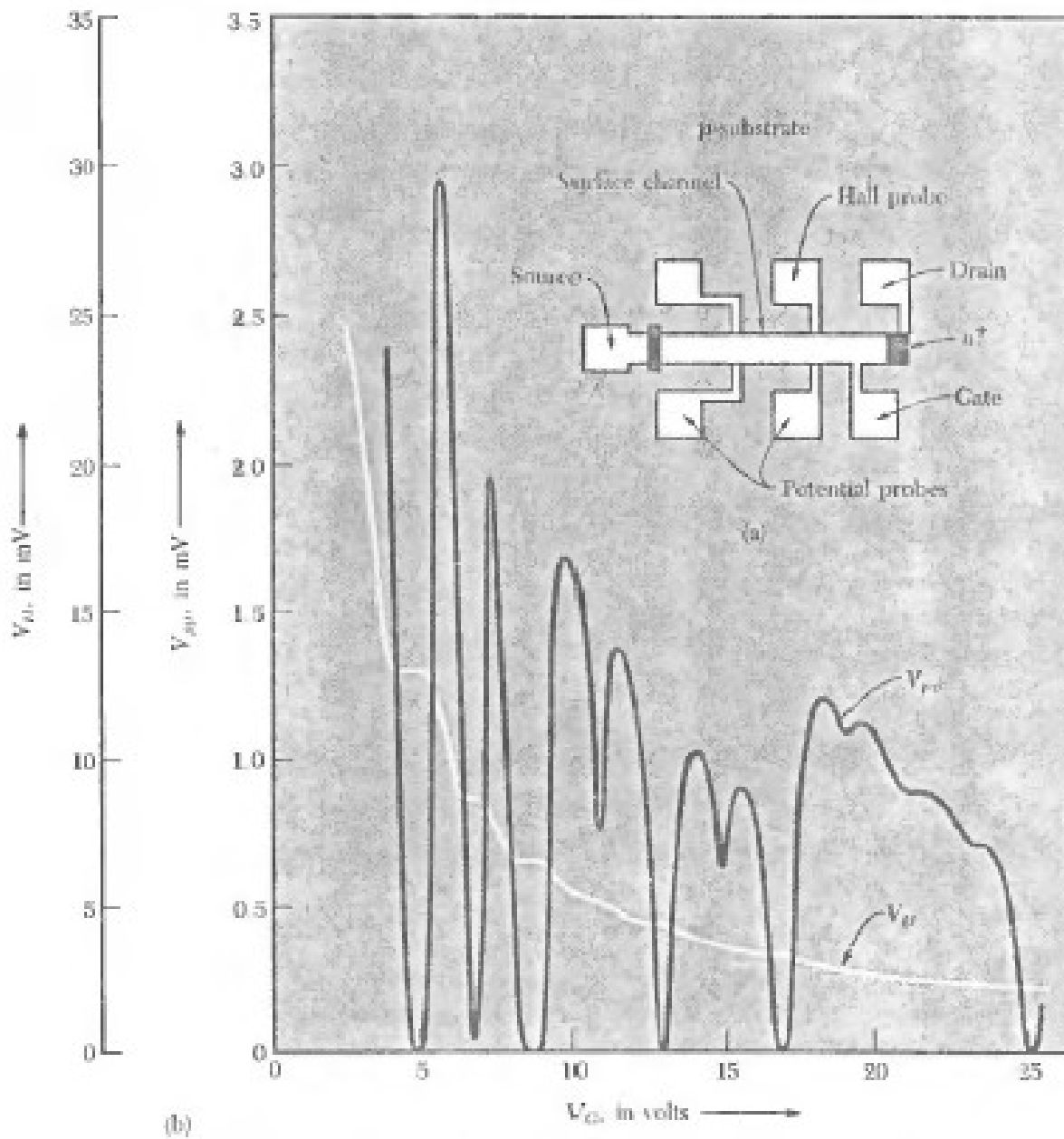
$$\rho_H = V_H / I = h / Ne^2$$

$$\rho_H = 25812,8075 / N \text{ k}\Omega$$



Kittel,
Introduction
to solid state
physics,
Wiley, 2005

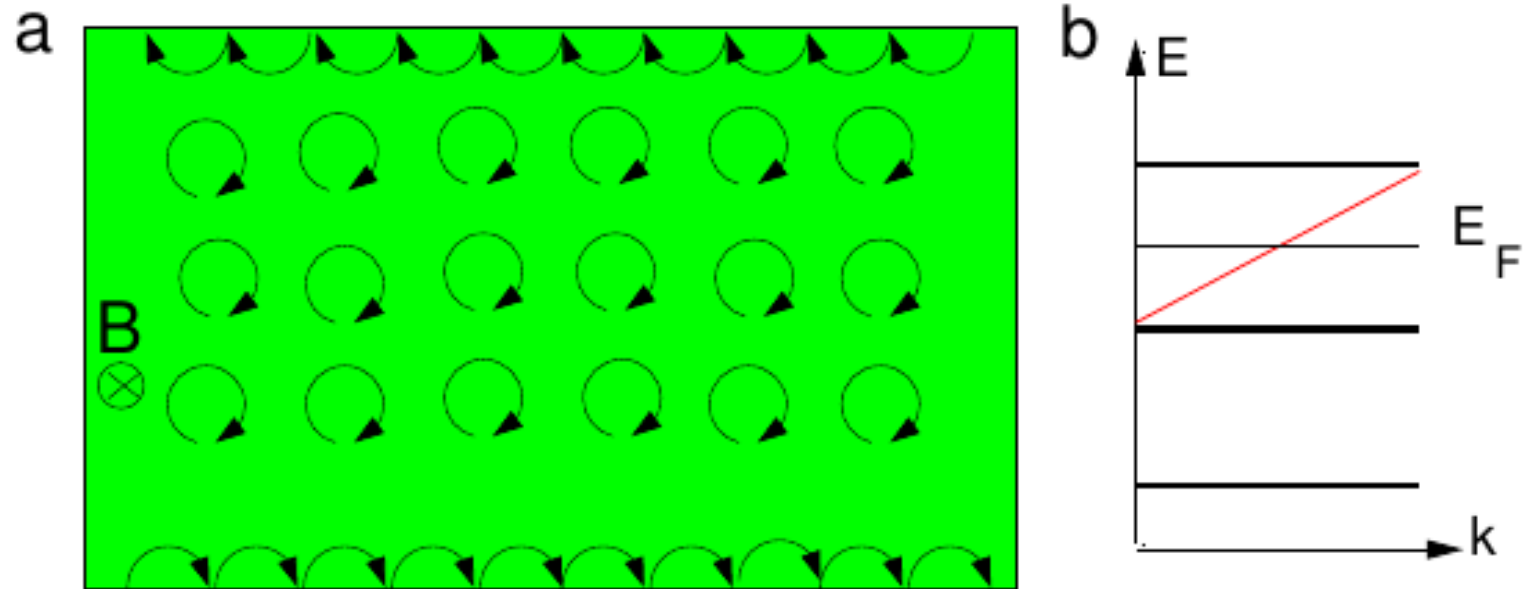
Kvantový Hallův jev – 2D elektronový plyn



K. von Klitzing, G. Dorda, M. Pepper, Phys. Rev. Lett. 45, 494 (1980).

Kvantový Hallův jev – 2D elektronový systém

Vysvětlení: elektrony v silném magnetickém poli Landauovy hladiny



$$\hat{\rho} = \begin{pmatrix} 0 & -\rho_{xy} \\ \rho_{xy} & 0 \end{pmatrix}, \quad \hat{\sigma} = \begin{pmatrix} 0 & \sigma_{xy} \\ -\sigma_{xy} & 0 \end{pmatrix}, \quad \sigma_{xy} = \nu \frac{e^2}{h}.$$

$$\rho_{xy} = \frac{V_{xy}}{I} = \frac{1}{\nu} \frac{h}{e^2} = \frac{1}{\nu} 25812.807 \Omega,$$

Metody měření magnetických vlastností

vibrační magnetometr

SQUID

Magnetooptický Kerrův jev (Faradayův)

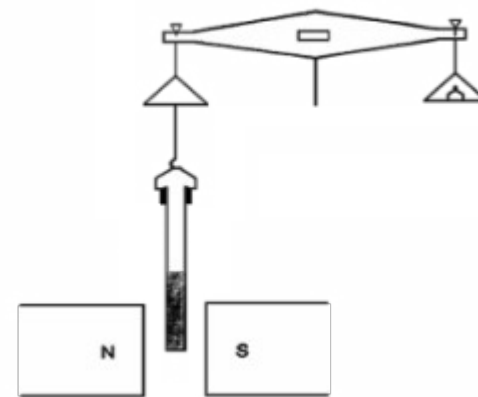
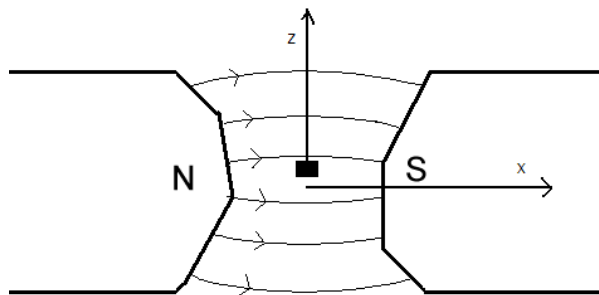
magnetický cirkulární dichroismus

XMCD

indukční magnetometrie

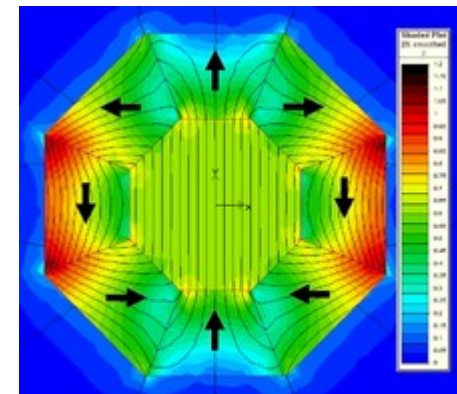
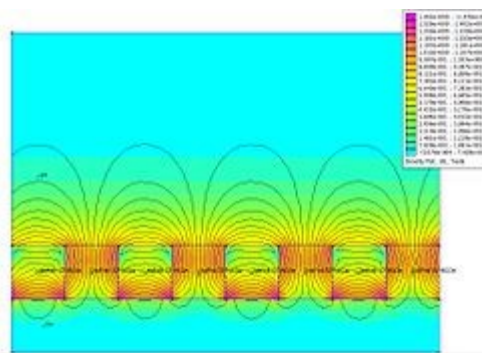
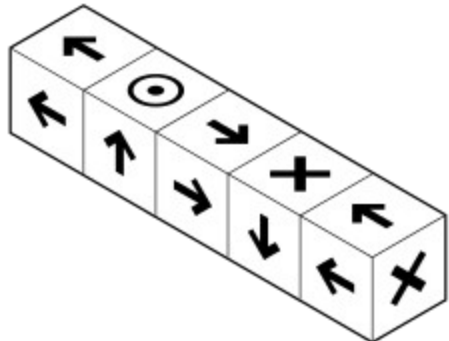
...

Faradayovy váhy - Gouyovy váhy



Metody získávání magnetických polí

Permanentní magnety do cca 1T
speciální konfigurace až 5T -- Halbachovo uspořádání



Rezistivní magnet s feromagnetickým jádrem max cca 2T - omezeno saturační magnetizací jádra

Supravodivý magnet (max cca 20T) - žádné rezistivní ztráty, nutnost kryogenních teplot

rezistivní magnet - vysoké rezistivní ztráty, nutné výkonné chlazení

kombinace supravodivého (vnější) a rezistivního magnetu.

Pulsní magnety -- krátkodobé